Integrated Ocean Drilling Program
Expedition 328 Preliminary Report

Cascadia subduction zone ACORK observatory

5–18 September 2010

E.E. Davis, M.J. Malone, and the
Expedition 328 Scientists and Engineers

Published by
Integrated Ocean Drilling Program Management International, Inc.,
for the Integrated Ocean Drilling Program

Publisher's notes

Citation:

E.E. Davis, M.J. Malone, and the Expedition 328 Scientists and Engineers, 2010. Cascadia subduction zone ACORK observatory. *IODP Prel. Rept.,* 328. doi:10.2204/iodp.pr.328.2010

Distribution:
Electronic copies of this series may be obtained from the Integrated Ocean Drilling Program (IODP) Scientific Publications homepage on the World Wide Web at **www.iodp.org/scientific-publications/.**

This publication was prepared by the Integrated Ocean Drilling Program U.S. Implementing Organization (IODP-USIO): Consortium for Ocean Leadership, Lamont Doherty Earth Observatory of Columbia University, and Texas A&M University, as an account of work performed under the international Integrated Ocean Drilling Program, which is managed by IODP Management International (IODP-MI), Inc. Funding for the program is provided by the following agencies:

National Science Foundation (NSF), United States

Ministry of Education, Culture, Sports, Science and Technology (MEXT), Japan

European Consortium for Ocean Research Drilling (ECORD)

Ministry of Science and Technology (MOST), People's Republic of China

Korea Institute of Geoscience and Mineral Resources (KIGAM)

Australian Research Council (ARC) and New Zealand Institute for Geological and Nuclear Sciences (GNS), Australian/New Zealand Consortium

Ministry of Earth Sciences (MoES), India

Disclaimer

November 2010

Expedition 328 participants

Expedition 328 scientists

Earl Davis
Chief Scientist
Pacific Geoscience Centre
Geological Survey of Canada
9860 West Saanich Road
Sidney BC V8L 4B2
Canada
edavis@nrcan.gc.ca

Mitchell Malone
Expedition Project Manager/Staff Scientist
Integrated Ocean Drilling Program
Texas A&M University
1000 Discovery Drive
College Station TX 77845-9547
USA
malone@iodp.tamu.edu

Martin Heesemann
Scientist
Pacific Geoscience Centre
Geological Survey of Canada
9860 West Saanich Road
Sidney BC V8L 4B2
Canada
martin.heesemann@nrcan.gc.ca

Michael Riedel
Scientist
Pacific Geoscience Centre
Geological Survey of Canada
9860 West Saanich Road
Sidney BC V8L 4B2
Canada
mriedel@nrcan.gc.ca

David Divins
Observer
Consortium for Ocean Leadership
1201 New York Ave Northwest, Fourth Floor
Washington DC 20005
USA
ddivins@oceanleadership.org

Education and Outreach: School of Rock

Jennifer Collins
Instructor
Consortium for Ocean Leadership
1201 New York Avenue Northwest, Fourth Floor
Washington DC 20005
USA
jcollins@oceanleadership.org

Kris Ludwig
Instructor
Consortium for Ocean Leadership
1201 New York Avenue Northwest, Fourth Floor
Washington DC 20005
USA
kludwig@oceanleadership.org

Steve Hovan
Instructor
Department of Geoscience
Indiana University of Pennsylvania
114 Walsh Hall
Indiana PA 15705
USA
hovan@iup.edu

Mary Reagan
Instructor
Lamont-Doherty Earth Observatory
Columbia University
PO Box 1000, Route 9W
Palisades NY 10964
USA
mreagan@ldeo.columbia.edu

Scott Slough
Instructor
Department of Teaching, Learning, and Culture
Texas A&M University
Mail Stop 4232
College Station TX 77843
USA
sslough@tamu.edu

James Brey
Participant
American Meteorological Society
1120 G Street Northwest, Suite 800
Washington DC 20005
USA

Patrice Ceisel
Participant
Ceisel & Associates, Inc.
1715 West Gregory Street
Chicago IL 60640
USA
pceisel@ceisel.com

Diane DeBaise
Participant
Commonwealth Connections Academy
4050 Crums Mill Road, Suite 303
Harrisburg PA 17112
USA
ddebaise0357@gmail.com

Don Duggan-Haas
Participant
PRI & Its Museum of the Earth
1259 Trumansburg Road
Ithaca NY 14850-1398
USA
dugganhaas@gmail.com

David Edwards
Participant
School of Public Policy and Professional Practice
Keele University
Staffordshire ST5 5BGE
United Kingdom
eseu@keele.ac.uk

Patti Gallagher-Jones
Participant
Honolulu HI 96826
USA
pgj500@yahoo.com

Kenneth W. Hamner
Participant
Smoky Hill High School
16100 East Smoky Hill Road
Aurora CO 80015
USA
khamner@cherrycreekschools.org

Sabreena Kasbati
Participant
Aquarium of the Pacific
100 Aquarium Way
Long Beach CA 90802
USA
teatgtts@aol.com

Jill Katzenberger
Participant
Denver Museum of Nature and Science
2001 Colorado Boulevard
Denver CO 80205
USA
jillykatz@gmail.com

Bob King
SOR Participant
Friendship Christian School
5400 Coles Ferry Pike
Lebanon TN 37087
USA
bobkingnesta@gmail.com

Maria Lazo
Participant
Brazos Valley Museum of Natural History
3232 Briarcrest Drive
Bryan TX 77802
USA
riaisland@hotmail.com

Kimberly Novak
Participant
Madison High School
5740 US Highway 25/70
Marshall NC 28753
USA
klnovak@mac.com

Emily Powell
Participant
Consortium for Ocean Leadership
1201 New York Ave Northwest, Fourth Floor
Washington DC 20005
USA
epowell@oceanleadership.org

Jean-Noel Puig
Participant
College Marguerite de Navarre
1 cours Bosquet BP
1514 Pau Cedex
France
jnhjpuig@wanadoo.fr

Andrea Swensrud
Participant
KQED Public Media
2601 Mariposa Street
San Francisco CA 94110
USA
aswensrud@kqed.org

John Van Hoesen
Participant
Green Mountain College
One College Street
Poultney VT 05764
USA
vanhoesenj@greenmtn.edu

Amy Work
Participant
Institute for the Application of Geospatial Technology
199 Franklin Street, Suite 300
Auburn NY 13021
USA
amwork@iagt.org

Technical support

Robert Aduddell
Engineer

Grant Banta
Marine Computer Specialist

Heather Barnes
X-ray Laboratory

Etienne Claassen
Marine Instrumentation Specialist

David Fackler
Marine Computer Specialist

Cesar Flores
Marine Computer Specialist

Ron Grout
Operations Superintendent

Ted Gustafson
Downhole Tools/Thin Sections Laboratory

Bradley Julson
Laboratory Officer

Jan Jurie Kotze
Marine Instrumentation Specialist

Koki Matsuo
Engineer

Erik Moortgat
Underway Geophysics Laboratory

Yasuhiro Namba
Engineer

Chieh Peng
Assistant Laboratory Officer

Steve Prinz
Assistant Laboratory Officer

William Rhinehart
Engineer

Kerry Swain
Logging Engineer

Acknowledgments

The Scientific Party of Integrated Ocean Drilling Program (IODP) Expedition 328 would like to express their appreciation to the IODP shipboard technical, operations, and engineering personnel and shore-based support staff. Master Terry Skinner, the Transocean officers, and the crew on the R/V *JOIDES Resolution* provided exceptional shipboard service. We benefited during Expedition 328 from the hard work, ingenuity, experience, and good humor of these multitalented personnel. We are particularly grateful for the concerted effort from Transocean rig floor personnel and IODP technical and engineering staff that allowed rapid assembly and trouble-free emplacement of the Advanced CORK (ACORK). Support for the design and construction of the wellhead instrumentation prior to the expedition was provided by Robert Macdonald, Robert Meldrum, James Guenther, John Bennest, Jonathan Schmidt, and David Miles.

A Cascadia ACORK caper

Two decades have passed since a beer-prompted brainstorm
To plug holes in the ocean that leaked every rainstorm.
CORKs they were called, and corking they did
Very well; seafloor Champagne was kept under lid.

Until one October, the weather was rough…
It made that first trip here frustratingly tough.
Formation squeezed in, the seal was broken
Now we've come back again, trepidation unspoken.

In the years that have passed we've found some new tricks
We can use to decipher our subduction fault's ticks.
Seafloor spreading won't stop, nor chronic plate motion,
But we'll watch as things happen down under the ocean.

Cascadia's fault is building up stress,
Squeezing water from rock, doing things not yet guessed.
But please not the big 'quake, we're not ready for that
Let's all cross our fingers for a long-delayed snap.

Now a toast: To the JR, always eager, on call,
To the funders who trust us to not drop the ball,
To NEPTUNE, the sea god who'll give us some power
And time syncs more frequent than once every hour,
To the schedulers who found us a window of time
For our little CORK caper, no cores, how sublime!

Abstract

The operational objective of Integrated Ocean Drilling Program Expedition 328 was the installation of a new permanent hydrologic borehole observatory near Ocean Drilling Program Site 889. The format of the new installation followed the Advanced CORK design, which will facilitate pressure monitoring at multiple formation levels on the outside of a 10¾ inch casing string. The observatory was successfully installed during the expedition and will allow documentation of the average state of pressure in the frontal part of the Cascadia accretionary prism, the pressure gradients driving flow from the consolidating sediments, the mode of formation of gas hydrates, the influence of gas hydrates and free gas on the mechanical properties of their host lithology, the response of the material to seismic ground motion, and the magnitude of deformation at the site caused by secular strain and episodic seismic and aseismic slip in this subduction setting. The casing was sealed at the bottom, leaving the inside available for future installation of additional monitoring instruments. At a later date, the observatory will be connected to the NEPTUNE Canada fiber-optic cable for power and real-time communications from land.

Introduction

Operations carried out during Integrated Ocean Drilling Program (IODP) Expedition 328 were devoted to the installation of a hydrologic observatory near Ocean Drilling Program (ODP) Site 889, the location chosen for a CORK (circulation obviation retrofit kit) observatory installation during ODP Leg 146 in 1992 (Westbrook, Carson, Musgrave, et al., 1994; Davis et al., 1995). In that early attempt, the relatively unstable sediments of the formation rapidly intruded through the perforations and bottom of an open-ended casing liner and prevented proper sealing of the hole. The new installation utilizes the Advanced CORK (ACORK) design, developed initially for installations at the Nankai subduction zone during ODP Leg 196 to permit pressure monitoring at multiple formation levels on the outside of a 10¾ inch casing string. The casing is sealed at the bottom, leaving the inside available for future installation of additional monitoring instruments.

A broad range of objectives will be addressed with monitoring over the decades to follow, some the same as those to have been addressed by the installation at Site 889, including documenting the average state of pressure and the vertical component of fluid flow from the consolidating sediments in the frontal part of the Cascadia accre-

tionary prism and investigating the mode of formation of gas hydrates. Other objectives have been added subsequently as a result of the multiple discrete monitoring levels provided by the ACORK configuration, advances in measurement resolution, and knowledge gained from other monitoring experiments. These include determining the influence of gas hydrates and free gas on the mechanical properties of their host lithology, the response of the formation to seismic ground motion, and the magnitude of strain at the site caused by episodic seismic and aseismic slip in this subduction setting. Instrumentation deployed at the time of drilling includes autonomously recorded seafloor and formation pressure sensors and seafloor temperature sensors. Sensors planned for deployment inside the sealed casing at a later date will measure temperature, tilt, and seismic ground motion. It is planned that all instruments will soon be connected to the NEPTUNE-Canada fiber-optic cable for power and real-time communications from land. This will permit sensor sampling rates, time accuracy, and monitoring lifetime that are much greater than would be possible with autonomous operation using battery power and locally stored data. The program grew from an ODP Letter of Intent submitted by E. Davis and Roy Hyndman and IODP Ancillary Project Letter 734 by E. Davis and Keir Becker.

Geologic context

IODP Site U1364 lies roughly 20 km landward of the toe of the Cascadia subduction zone accretionary prism, where much of the thick section of turbidite and hemipelagic sediments deposited on the eastern flank of the Juan de Fuca Ridge are scraped off the underthrusting oceanic crust (Fig. **F1**). Convergence of the Juan de Fuca oceanic plate relative to the North American continental plate occurs in a direction roughly normal to the continental margin and at a rate of roughly 42 mm/y (DeMets et al., 1990). A topographic trench at this subduction zone is absent as a consequence of the extremely high rate of glacial sediment supply from the continent during the Pleistocene. The majority of the supply has been impounded by the elevated igneous crustal topography of the Juan de Fuca Ridge to form what is called Cascadia Basin. At the accretionary prism toe (also referred to as the deformation front, where the thrust-fault interplate interface intersects the seafloor), the sediments of Cascadia Basin are >2 km thick; at Site U1364 the accreted sedimentary section is roughly twice this thickness (Fig. **F2**). With tectonic thickening and compaction, pore fluids are expelled, and gas—primarily biogenic methane—is transported upward to contribute to the formation of gas hydrates in the upper few hundred meters of the sediment section. The location for Site U1364 was chosen on the same basis as that for Site 889. It

lies at a position landward of the prism toe where the fluid expulsion rate, estimated on the basis of the rates of compaction and vertical growth of the prism, reaches a cross-margin maximum and where a clearly developed bottom simulating reflector marks the base of the gas hydrate stability field (Davis et al., 1990). Other holes drilled earlier during ODP Leg 146 and IODP Expedition 311 (Westbrook, Carson, Musgrave, et al., 1994; Riedel, Collett, Malone, et al., 2006) documented the nature of the incoming undeformed sediments, the compaction history during accretion, the details of the sediment lithology, and the distribution and composition of gas hydrates across the area. This information, along with extensive site survey studies (Schwerwath et al., 2006; Riedel et al., 2010) provided an excellent basis for planning the depth, location, and other details of the ACORK installation at Site U1364 and will provide a valuable context for anticipated ACORK observations.

Seafloor morphology in the vicinity of Site U1364 (Fig. **F3**) reveals an active and heterogeneous accretional, depositional, and erosional geologic regime. The deformation front/prism toe is marked by uplifted anticlinal ridges, thrust fault traces, and local slope failures with accompanying debris deposits on the adjacent Cascadia Basin abyssal plain. In several places, the uplifted frontal structures are cut by canyons that funnel gravity-driven sediment transport from sources higher on the continental slope and outer shelf. Large scours and sand waves can be seen where these empty into Cascadia Basin. Headless canyons are common high on the slope, terminating at the shelf-slope break.

A closer look in the area of Site U1364 (Fig. **F4**) shows seafloor manifestations of focused fluid discharge. Seafloor seeps and vents discharge water expelled from the thickening prism, and in many instances free gas is transported across the 250 m thick zone of gas hydrate stability by relatively rapid focused upward flow. No vents have been observed in the immediate vicinity of Site U1364, but those that are present in the area (e.g., "Bullseye vent" and other locations where pock-marks, carbonate mounds, and gas hydrates are present at the seafloor) demonstrate that super-hydrostatic pore-fluid pressure and free gas are present beneath the seafloor.

A simplified schematic cross section in Figure **F5** illustrates one way gas hydrates are believed to accumulate in accretionary prisms. Pore-fluid expulsion, driven by tectonic thickening and consolidation, is rapid near the prism toe and diminishes landward. Vertical migration of water from the prism delivers small amounts of dissolved methane produced in the sediment by biological CO_2 reduction to the level of gas hydrate stability (a weak function of pressure and strong function of temperature),

where gas hydrates accumulate primarily in permeable fractures and coarse-grained layers. The boundary between sediments containing free gas and sediments containing gas hydrate in the sediment pore volume may be enhanced as a result of methane recycling at the phase boundary from vertical tectonic motion, sedimentation, and erosion (Haacke et al., 2007). This boundary is seen in seismic profiles throughout the Site U1364 area as a bright reflection (the bottom-simulating reflector) at a generally uniform depth below the seafloor (a consequence of its depth being primarily temperature controlled), with a polarity opposite to that from the seafloor (Fig. **F6**).

Seismic reflection profiles crossing Site U1364 (Fig. **F6**) (Riedel, 2001) also provide a clear image of the local sediment structure, which comprises a gently deformed sequence of slope-basin deposits draped over highly deformed accretionary prism sediments. Accreted and deformed sediment occurs close to the seafloor or in outcrop in the high-standing area southeast of Site U1364 (Fig. **F4**); this lithology plunges northwest and is buried by a veneer of gently deformed locally deposited slope-basin sediments roughly 100 m thick at the location of Site U1364. These lithologic units have been characterized in detail by coring and logging at the numerous holes drilled in the immediate vicinity of Site U1364 (Fig. **F4**) (Westbrook, Carson, Musgrave, et al., 1994; Riedel, Collett, Malone, et al., 2006; Riedel et al., 2010; see next section). The gas/gas hydrate interface responsible for the extensive bottom-simulating reflector was intersected by these holes at a depth of roughly 225 meters below seafloor (mbsf), well within the deformed prism unit. Gas hydrates above the interface appear to be virtually absent in fine-grained sediments; most of the gas hydrate is concentrated in permeable coarse-grained units and massive gas hydrate lenses that mark present or past pathways of focused fluid flow.

Lithostratigraphy at Site U1364

Site 889

Core and log data from Site 889 showed three major lithostratigraphic units within the uppermost 400 mbsf. Lithostratigraphic Unit I was divided into Subunits IA and IB. Subunit IA (seafloor to 87 mbsf in Hole 889A) comprises mostly clayey silts and silty clays with interbedded thin sand layers. This unit is characterized by subhorizontal to gently dipping beds with little deformation and was interpreted to be turbidites and pelagic sediments deposited in a slope basin. Subunit IB (91–128 mbsf in Hole 889A) is also mainly silty clay but with fewer sand layers. It was interpreted that the

sediments in Subunit IB represent a series of sediment gravity flow deposits caused by tectonic uplift at the deformation front and thus a transition between the abyssal plain sedimentation of lithostratigraphic Units II and III to the subsequent deposition of Subunit IA, which represents slope basin sedimentation.

Units II and III consist of mainly clayey silt with a low abundance of sand layers and are distinguished only by an increase in glauconite in Unit III. No structural differences between these two units were observed. They were interpreted as typical abyssal plain sediments that were heavily deformed and fractured during the accretion process. Seismic profiles show that Subunit IB has also suffered deformation, and the boundary between accreted and slope sediments was placed at ~90 mbsf within Unit I.

Site U1327

Five holes were drilled at Site U1327 (Riedel, Collett, Malone, et al., 2006), and the section was divided into three main lithostratigraphic units that differ from those defined at the time of Leg 146. Unit I (0–90 mbsf; age <0.3 Ma) comprises dark greenish gray and dark gray clay and silty clay, often interbedded with silt, clayey silt, sandy silt, sand, and gravel layers. It is characterized by fine-grained detrital sediments (clay and silty clay) with abundant coarse-grained layers as thick as 6 cm that indicate turbidity flow deposition. Some carbonate cement is present. The boundary between Units I and II is marked by a sharp decrease in sand and silt layers and a sharp increase in the abundance of diatoms. The average rate of sedimentation was estimated to be 22 cm/k.y.

Lithostratigraphic Unit II (90–170 mbsf; age >0.3–1.0 Ma) comprises dark greenish gray and dark gray clay; clay with diatoms; and silty clay, silty clay with diatoms, and diatom silty clay locally interbedded with sandy silt and sand layers and lenses. Very few carbonate cements are present. Soupy and mousselike sediment textures correlated with cold sections in the core imaged with an infrared scanner; these were inferred to be the consequence of the dissociation of interstitial gas hydrate during recovery. The average sedimentation rate for Unit II is estimated at ~16 cm/k.y. Intervals with a high ratio of nonmarine versus marine diatoms indicate an increased contribution of terrigeneous detrital sediments from land sources by turbidites. The great abundance of marine diatoms along with spores suggests initial deposition beneath a coastal upwelling environment followed by reworking by turbidity currents.

Lithostratigraphic Unit III (170–300 mbsf; age >1 Ma) comprises dark greenish gray and dark gray silty clay, with some exotic rock clasts. Diatoms are absent immediately below the Unit II/III boundary, although diatoms reappear below 248 mbsf. Unit III is distinguished from Unit II by a higher degree of induration of the sediments compared to lithostratigraphic Unit II. Carbonate cements are rare. The depositional environment for Unit III was interpreted to have been dominated by low-energy turbidity currents in an abyssal plain environment. The biostratigraphically estimated average sedimentation rate in this section is 12 cm/k.y.

Site U1327 logging data

Physical property variations defined by logging at Site U1327 (Fig. F7) do not reflect the lithostratigraphy described above in any obvious way, but they provide valuable contextual information about the section spanned by the Site U1364 ACORK. General trends of increasing bulk density, electrical resistivity, and sonic velocity and decreasing porosity with depth are defined, with porosity ranging from roughly 0.7 at the seafloor (measured on cores) to ~0.50 at 300 mbsf. A major anomaly is seen in the logging-while-drilling (LWD) data between 120 and 145 mbsf. This is inferred to reflect a localized massive hydrate horizon (defined only in Hole U1327A). At 230 mbsf, a decrease in resistivity is seen in the resistivity logs and the resistivity-at-the-bit (RAB) image, as are sharp decreases in density and sonic velocity and an increase in porosity. These changes, and the change in character of the RAB image, are consistent with gas hydrates being present in discrete layers above 230 mbsf and gas being present below. The ACORK screens are distributed roughly symmetrically around this boundary; screens 1 and 2 lie at 74 and 14 m below and screens 3 and 4 lie at 27 and 74 m above the boundary, respectively.

Seismotectonic context

Much of the motivation for establishing a borehole observatory at Site U1364 derives from a need to understand the nature of deformation across the full width of a subduction zone like Cascadia that hosts infrequent but very large (Mw ~9) earthquakes generated along the subduction thrust interface. Recent events include Kamchatka (1952), southern Chile (1960), eastern Aleutians (1964), and Sumatra (2004). The most recent “megathrust” earthquake at Cascadia is known from tsunami records in Japan to have taken place in 1700 (Satake et al., 1996), and the interval between large events estimated from sequences of tsunami deposits in coastal and offshore areas

ranges from 200 to 800 y (Goldfinger et al., 2003; Leonard et al., 2010). Very large subduction earthquakes are known to be generated by rupture propagating along segments ~1000 km long, but the precise width and position of the seismogenic rupture surface is only modestly well constrained. Updip and downdip limits of rupture are controlled by factors including rock mechanical properties (influenced by temperature and composition), fluid pressure, and interface roughness; observationally, the limits are typically estimated on the basis of seismic radiation patterns of great earthquakes and vertical and horizontal coseismic and postseismic deformation where it can be measured in adjacent subaerial areas. Slow interseismic deformation also provides information about seismogenic deformation, as they are very approximate mirror images of one another. The zone of seismic coupling is offshore in most subduction zones, so constraints from land-based observations provide an incomplete and biased view; observations like those to be made at Site U1364 are bound to add invaluable insight into both interseismic and seismogenic behavior of subduction zones. We anticipate that slow interseismic strain accumulation may be resolved, and it is possible that aseismic deformation events may be present, as have been observed along the subduction thrusts at Costa Rica (Davis and Villinger, 2006; Davis et al., submitted) and the Nankai Trough (Davis et al., 2009) (e.g., Fig. **F8**).

In addition to the Cascadia subduction zone being host to occasional giant thrust earthquakes, local plate motions generate frequent earthquakes with smaller magnitudes (Fig. **F9**). To the northwest of Site U1364, strike-slip events are concentrated along the Nootka fault, the strike-slip boundary between the Juan de Fuca and Explorer oceanic plates. Along the continental margin, intraplate events occur within the overriding continental crust and within the oceanic crust of the subducting Juan de Fuca and Explorer plates (Fig. **F9A**). Further landward, seismic tremor occurs episodically along and above the top of the subducting plate, downdip of the thrust seismogenic zone (Kao et al., 2009) (Fig. **F9B**). Strain associated with local seismic events is known to be detectable as pressure transients (e.g., Fig. **F10**), and the comparison of the strain estimated from pressure with the strain estimated from seismic moments will provide invaluable information about seismic rupture processes in the oceanic crust and upper mantle, the continental crust, and the more consolidated parts of the accretionary prism. The possible frequency of occurrence of events that can be resolved in the CORK pressure records at Site U1364 is illustrated in Figure **F11,** which shows the seismic recurrence relationship for the region around the drill site. The known sensitivity to strain produced by earthquakes of magnitudes as low as Mw = 5 at a range of up to 100 km (Fig. **F10**) suggests that strain transients of one or more events per year should be resolved at Site U1364.

Beyond these scientific considerations, a number of technical factors added to the motivation to establish a geophysical observatory at this site. High reliability of CORK instrumentation has been demonstrated through successful long-term operations at many sites. Instruments deployed during Leg 196 (Nankai Trough) have been operating for >8 y, and those deployed during ODP Legs 168 and 169 have been in operation for >13 y. Improvements in power consumption, memory capacity, and resolution now permit detection of much subtler signals than were previously possible. And in this instance, connection to the NEPTUNE-Canada cabled observatory infrastructure will open new opportunities. Much higher sampling frequency will be achieved, allowing observations to reach into the seismic frequency band (Fig. **F12**) and to be placed in the context of collocated seismic and hydrologic records that are currently being collected with a broadband seismometer and a variety of seafloor vent monitoring instruments roughly 3.5 km from the Site U1364 ACORK borehole observatory, as well as those that will be collected with additional instrumentation planned for Hole U1364A.

The Site U1364 ACORK observatory configuration

Background

Starting in the late 1980s, ODP engineers and scientists developed the CORK hydrologic observatory system to seal cased boreholes at the seafloor and allow the formation state to be monitored continuously for years after drilling (Davis et al., 1992). In 1991, the first CORKs were installed in two holes drilled through sediment and into igneous basement in the Middle Valley rift of the northernmost Juan de Fuca Ridge (Davis and Becker, 1994), with the goal of determining the natural hydrologic state of this hydrothermally active setting (i.e., after the large perturbations from drilling and open-hole conditions had dissipated). Other sites followed, including two in the Cascadia accretionary prism (Davis et al., 1995), two in the Barbados accretionary prism (Becker et al., 1997; Foucher et al., 1997), four on the eastern Juan de Fuca Ridge flank (Davis and Becker, 1998, 1999), one on the western Mid-Atlantic Ridge flank (Davis et al., 2000; Becker et al., 2001), and one in a Mariana forearc serpentinite diapir (Salisbury, Shinohara, Richter, et al., 2002; Wheat et al., 2008). Although the specific objectives of these installations have differed, all of the monitoring experiments have made use of the basic CORK capabilities to monitor seafloor and formation temperatures and pressures over long periods of time. Beginning with the Barbados installations, fluid samplers were added to some of the temperature sensor cables to allow

continuous sampling of deep-formation water. At several of the CORK sites, additional sampling and hydrologic testing experiments have been completed using valves that allow controlled access to the sealed sections (e.g., Screaton et al., 1995, 1997).

These original CORKs succeeded in preventing borehole flow, allowed formation pressures to be measured accurately, and allowed temperatures to be determined at multiple depths. However, use of only a single seal meant that the formation pressure observed and fluid samples collected reflected averages over the open sections of the holes (i.e., either the entire length of open hole beneath casing in igneous basement or the length of perforated casing within sediments). Determinations of local pressure gradients were not possible. This limitation, along with the success of the initial CORK design, stimulated interest in enhancing the capabilities to include monitoring of multiple zones in a single hole and to permit a greater range of sensor capabilities.

These objectives were addressed with the ACORK (Mikada et al., 2002; Becker and Davis, 2005), designed for a variety of applications and installed for the first time during Leg 196 for a long-term monitoring experiment in the Nankai subduction zone. Other variations of the CORK system followed (e.g., Jannasch et al., 2003; Becker and Davis, 2005; Fisher et al., 2005). All take greater advantage of individual boreholes by utilizing packers and screens to allow pressures to be observed at multiple levels, just as is often done in terrestrial hydrologic experiments. The ACORK system consists of a 10.75 inch outer diameter, 10.05 inch inner diameter casing string with modular screened monitoring elements positioned at desired depths. The initial ACORKs included hydraulically inflated packer elements to isolate screens, although experience from Nankai monitoring showed that collapse of the formation provided good hydrologic isolation in intervals where no packers were used and experience elsewhere demonstrated that hydraulically inflated packers were ineffectual for long-term use. Pressure monitoring and/or fluid sampling is done via a multiline hydraulic umbilical strapped to the outside of the casing. Hydraulic lines from each level pass successively through packers and screens above and are then plumbed into a seafloor framework that houses sampling and testing ports, pressure sensors, and data loggers. Once the casing with its packers and screens is in place and a bridge plug is installed to seal the casing at its deepest point, the inside of the ACORK string becomes hydrologically isolated from the formation. In this way, access to the hole inside the sealed casing is provided for downhole instruments to the total depth of the installation without perturbing the pressure monitoring.

Most CORK installations to date have been configured to meet a broad suite of requirements, including passive geophysical monitoring, active hydrologic testing, and formation-fluid chemical and microbiological sampling (see reviews by Kastner et al., 2006; Becker and Davis, 2005; Fisher et al., 2005). Unfortunately, large perturbations can occur when fluids are produced from the formation, particularly when monitoring screens are situated in low-permeability material. Direct effects arise from any pressure drop associated with production, and indirect effects arise from thermal perturbations caused by flow (see discussion in Davis and Becker, 2007). The latter can be caused by the anomalous buoyancy of the water in the umbilical that connects the screens to the seafloor sensors and from transient thermal expansion of the fluid in the umbilical and screens that is confined by the low-permeability material surrounding the screens. To avoid these problems, the observatory at Site U1364 will be devoted to passive geophysical monitoring exclusively; fluid sampling and other formation-interactive experiments devoted to gas hydrates are being planned in separate devoted holes roughly 3 km to the southeast.

Site U1364 ACORK details

The primary components of the ACORK system deployed in Hole U1364A are shown in Figs. F13–F16. Four screens are centered at 156.3, 203.2, 243.6, and 303.6 mbsf, two above and two below the gas/gas hydrate boundary at ~230 mbsf and all within the accretionary prism lithologic unit (Fig. **F7**). Details of the various components are described as follows:

Screens

Hydrologic access to the formation was provided by 2.03 m long screen filters on 6.08 m long casing joints (Fig. **F13**). Carbolite granulate is packed in a 1.55 cm annulus between the outside of a solid section of 10¾ inch casing and a screen formed of wire wrapped on radial webs. Hydraulic lines leading to deeper intervals pass straight through the filters. The monitoring line accessing each filter is perforated along its length within the corresponding screen. Carbolite, an aluminum oxide ceramic, was used for the filter fill, with a grain size of 400–800 µm, a porosity of ~30%, and a permeability of 5×10^{-10} m^2. The screen was wound with triangular 316 stainless steel wire with a surface width of 2.8 mm and a gap width of 0.4 mm, providing an effective open cross section of 12.5%. The design was intended to provide good hydrologic communication to the formation, with maximum effective contact area and perme-

ability, while preventing sediment from invading and clogging the sampling or monitoring lines.

Hydraulic tubing

Formation pressure signals are transmitted to seafloor sensors via ¼ inch outer diameter 0.035 inch wall 316 stainless steel hydraulic tubes laid in a flat format and jacketed with polyurethane to form a single, robust umbilical (Fig. **F14**). Swaged connections were made during deployment between the umbilical and the tubes leading through or from each screen. Unused tubes in each section of umbilical between screens were capped at their bottom ends to prevent hydraulic communication between screens and left open at their tops to prevent collapse and damage to the rest of the umbilical. The umbilical was banded to the outside of the casing sections at roughly 4 m intervals. The tubing was chosen on the basis of what was felt to be a reasonable compromise between hydraulic capacitance, resistance, and robustness. Capacitance and resistance of the formation (the inverse of the product of these being equivalent to the hydraulic diffusivity) are likely to be high in parts of the sediment section. Hence, to transmit pressure variations over a broad range of frequency with no distortion requires the observation system to have very low resistance and capacitance. The quartz pressure sensors are essentially incompressible, and the compressibility of the thick-walled tubing can also be ignored; the water filling the tubing is the primary source of the observing system compliance. Reducing the internal diameter of the tubing is advantageous in that lesser amounts of water are required to flow in and out of the formation to transmit pressure signals, but only up to the point when the translation of fluid begins to be frictionally influenced by the tube wall. Given expected formation signal amplitudes, the dimension of the tubing chosen is much larger than necessary; the limiting factor was the size that could be handled without fear of clogging with either fine sediment that might invade the screens or grease and constrictions at the tube joints that might occur at the time of deployment. A quantitative discussion of the transmission of signals in context of formation permeability is provided in Davis and Becker (2007).

Wellhead configuration

The ACORK head is a 30 inch diameter cylindrical frame fabricated from ⅜ inch steel around a section of 10¾ inch casing. It provides space for instruments, wiring, and plumbing in each of three 120° wide, 78 inch high bays bounded at the top and bottom by circular horizontal bulkheads and divided from one another by radial webs

(Fig. F15). All components are contained in a single bay in the Hole U1364A installation, including the sensor/logger/underwater-mateable connector assembly on its demountable frame and three-way pressure sensor valves (Fig. F16). The lowermost bulkhead is positioned ~16 inches above a submersible landing platform that covers the main 4.5 m diameter reentry cone. The ACORK running tool receptacle fitting at the top of the ACORK head doubles as a 23¾ inch diameter reentry funnel for bridge-plug and wireline instrument installations. A larger auxiliary reentry funnel was deployed to facilitate reentry into the 10¾ inch ACORK casing, but it failed to seat and fell to the seafloor after the bottom-hole assembly (BHA) was removed (see **"Operations summary"**).

Pressure monitoring instrumentation was installed in the wellhead frame on the ship and deployed with the ACORK casing string (Fig. F16). Pressure-balanced underwater-mateable hydraulic connectors allow the instrument package to be removed and replaced by submersible or remotely operated vehicle (ROV) in the event that repairs or service are ever required. Three-way valves connect the umbilical lines to the instrumentation. In the "interval" position, these connect the formation to the sensors; in the "seafloor" position, the formation lines are closed and the sensors are connected to the ocean, allowing periodic checks on drift. A critical step in the assembly operation of every deployment is to purge air from all lines. In quantities too large to be absorbed by the local volume of water, trapped air will greatly increase the compressibility of the system and thus reduce the fidelity of the response to high-frequency formation pressure variations. Purging is done through lockable check valves at the highest point of the wellhead plumbing by submersing the fully assembled ACORK system below the moonpool immediately prior to deployment. Lines and couplers between the sensors and the three-way valves were purged when the instrument system was mounted to the wellhead frame. Pressure tests were carried out to test against leakage; results of those tests are shown in Figure F17.

Sensors and logging electronics

The logging instrumentation includes individual sensors (Paroscientific 8B4000-2 and 8B4000-1 quartz depth sensors) to monitor pressures at the seafloor and at each of the formation screens (Table T1). Frequency signals from these sensors are digitized with high-resolution (~1 ppb frequency or 10 ppb full scale pressure = 0.4 Pa, equivalent to 0.04 mm of water head) low-power Precision Period Counter (PPC) cards (Bennest Enterprises, Ltd.). The records shown in Figure F17, collected during a plumbing leakage test prior to deployment, give a sense of measurement resolution.

Absolute accuracy is limited by sensor calibration and drift. Experience from previous multiyear deployments shows that drift is typically <0.4 kPa/y. Drift and calibration inaccuracy (~5×10^{-4} of total pressure or roughly 10 kPa at Site U1364) are dealt with by intergauge hydrostatic checks immediately prior to installation and later at times of submersible visits using the wellhead three-way valves. Bottom water temperature is measured by a temperature-sensitive quartz oscillator of one of the Paroscientific sensors, as well as with a highly stable platinum thermometer. Time-tagged frequency and temperature data are stored by a MT-01 (Minerva Technologies, Ltd.) data logger that utilizes a low-power SanDisk 512 megabyte flash memory card. On-board power is supplied by 12 DD lithium-ion batteries having a total capacity of 210 A-h, sufficient to power the system for roughly 10 y at a sampling period of 1 min (user programmable). An onboard voltage detection circuit will automatically switch the system into a high-rate (1 Hz) sampling mode and idle the batteries when external power from a NEPTUNE connection is made (anticipated within the first year of operation). Serial RS422 communications with the instrument and an external power feed is accommodated via a seven-contact Teledyne ODI underwater-mateable connector (Fig. **F16**). The instrument pressure case is built of 4130 alloy heat-treated steel, pressure tested for use to a 2800 m water depth following deep submersible research vessel (DSRV) *Alvin* certification specifications. The total weight of the instrument assembly is ~43 kg in water.

Other downhole instruments planned for future installations will be wireline-deployed inside the 10¾ inch casing using a submersible or remotely operated vehicle. These will include a thermistor cable, tilt sensors, and a seismometer.

Data format and calibration

The CORK's MT-01 data logger is configured to make real-time data from the RTC/PPC (real-time clock + controller/precision period counter) measurement system available via an RS-422 serial interface and concurrently to store all readings in memory. Data transmission rates for real-time access as well as data download are configured to be 115,200 baud. Parameter files documenting the instrument's configuration can be reviewed at the CORK Observatory Software repository (**www.corkobservatories.org/**). Software packages mentioned below can also be downloaded.

An example of the real-time data as it will be received by NEPTUNE Canada once a cable connection is established is provided in Table **T2.** Binary data records, containing a timestamp, the logger ID, the logger housing temperature, the readings from the

pressure sensors, and a trailing zero byte, are written to compact flash memory. These are converted to hexadecimal and sent to the RS-422 interface as lines of ASCII characters.

Data stored in the logger can be downloaded using a conventional communications terminal program, but for speed and ease of use reasons we highly recommend the use of the "mlterm" software available at the Web site given above. The downloaded *.raw files contain the complete custom file system of the logging unit, which must be stripped from the data records prior to any further processing. This is done using the "mlbin" software also available from the Web site.

Given the complex CORK setup, with four Type I (pressure only) and one Type II (pressure and temperature) Paroscientific pressure sensors, the "mldat" software that is usually used to convert raw data to engineering units cannot be used. Python code, which can handle the necessary calibrations of more complex CORK setups, was developed for this purpose (see the CORK Observatory Software repository). To ensure the usability of the data in the future, all necessary information to convert the raw data to engineering units is given below:

Timestamp (4 bytes)

Times are recorded in seconds since 1-Jan-1988 00:00:00.

Logger ID (1 byte)

The ID (08) is the hexadecimal representation of the ID byte; it is associated with the RTC electronics.

Internal temperature (logger housing) temperature (3 bytes)

The logger/RTC/PPC pressure housing temperature is measured using a platinum sensor mounted to one endcap with thermal contact compound. The conversion from readings (x) to housing temperatures (T_h) in degrees Celsius is done using

$T_h = a * x + b.$

For the sensor used (serial number 92), the calibration coefficients are a = –2.95416e–006°C and b = 40.1418°C.

Pressure sensor temperature (4 bytes)

Pressure sensor temperature data are recorded for the seafloor sensor. The sensors for the formation are capable of recording only pressures; this provides enhanced pressure resolution, reduced power consumption, and reduced stored data quantity. The conversion of AD counts x_{TF} from the pressure sensor temperature channel is done in three steps. First, the counts are converted into the period X (µs) of the temperature oscillator (a conversion that is the same for all PPC measurement devices):

$X = (x_{FT} + 4294967296)\ (4.656612873e{-}9/4)\ \mu s.$

In a second step, the difference U between the measured period X and the period U0 at 0°C is computed:

$U = X - U_0.$

U_0 is a calibration coefficient that differs for each pressure sensor (Table **T3**). The differential period U is used to compensate the pressure channel of the same sensor (see below) and to compute the sensor temperature (T_p) using the calibration coefficients Y_i (Table **T3**):

$T_p = Y_1U + Y_2U^2.$

Formation pressures (4 × 4 bytes)

Formation pressures measured at screen #1 (deepest) to screen #4 (shallowest) are measured using Type I Paroscientific pressure sensors (no temperature-dependent frequency signal). For the temperature compensation of the pressure signal from these sensors, an external temperature measurement must be supplied. For this purpose, we use the temperature measured by the seafloor pressure sensor, which is collocated with the other pressure sensors and should have a similar thermal time constant. From our experience, the logger pressure housing temperature has a much smaller time constant than the pressure sensors—the quartz oscillators (both pressure and temperature) are by design thermally well isolated within the Paroscientific pressure sensor housings. Therefore, use of the logger housing temperature for temperature compensation would induce high-frequency noise in the calculated pressures. For Type I sensors, the compensation factor U equals the temperature in degrees Celsius we wish to compensate for. Otherwise, the same calibration procedure as for Type II sensors (see below) applies.

Seafloor pressure (4 bytes)

The seafloor pressure sensor is the only Paroscientific Type II sensor (temperature and pressure channel) of the CORK. The temperature compensation factor U for this sensor is the differential period $X - U_0$ and not the temperature in degrees Celsius as for Type I sensors (see above). If the temperature period for a Type II sensor is not available, U can be computed from an externally provided probe temperature T_p using the following equation (cf. Table **T3** for calibration coefficients):

$$U = -[Y_1 + \mathrm{sqrt}(Y_1^2 + 4\ Y_2\ T_p)]/(2\ Y_2).$$

Given a temperature compensation factor U, the conversion of logged PPC counts x_{PF} from a sensor pressure channel is done in three steps. First the counts are converted into periods τ (µs) of the pressure oscillator, a conversion that is the same for all PPC pressure channels:

$$\tau = 4.656612873e{-}9\ (x_{FP} + 4294967296)\ \mu s.$$

Next, a set of three compensation factors (C, D, and T_0) is computed based on the calibration coefficients C_i, D_i, and T_i, which are provided by Paroscientific Inc. for each pressure sensor (Table **T3**):

$$C = C_1 + C_2\ U + C_3\ U^2,$$

$$D = D_1,$$

and

$$T_0 = T_1 + T_2\ U + T_3\ U^2 + T_4\ U^3.$$

Finally, the temperature-compensated pressure P (in psia) is computed from the factors above:

$$P = C(1 - T_0^2/\tau^2)\ [1 - D(1 - T_0^2/\tau^2)].$$

To convert the compensated pressures into dBar or kPa, they must be multiplied by 0.6894757 dBar/psia or 6.894757 kPa/psia, respectively.

Trailing zero (1 byte)

As shown in Table T2, each sample record in the binary data is terminated by a zero byte. In the ASCII RS-422 output the records are terminated by carriage-return line-feed characters and thus appear on separate registered lines. The constant number of bytes between the ID byte and the trailing zero byte helps to identify the start and end points of data records, in the event that the structure of the binary data is disrupted (e.g., by incomplete data records).

Screen spacing

At the simplest level, the four monitoring points enumerated above will allow determinations of the average vertical pressure gradient generated by prism thickening and driving vertical fluid flow, along with the contrast in gradient between the section above and below the level of gas hydrate stability associated with a contrast in permeability if one exists. The combination of the 2.03 m length of the screens and their ~50 m separation should make such gradient determinations relatively insensitive to localized heterogeneities associated with fractures, turbidite layering, and lenses of massive gas hydrate accumulation.

Data from below and above the gas/gas-hydrate boundary will also constrain the contrast in mechanical properties of gas- and gas hydrate–bearing sediments and provide independent information about the effective permeabilities of the sections above and below the boundary. The way this can be done is summarized in Figure F18, which begins with a schematic illustration of how variable loading either at the seafloor (e.g., tides and ocean waves) or within the formation (tectonic strain and seismic waves) is transmitted to formation pore water and how local contrasts in loading response causes transient pressure gradients to be established (Fig. F18A). The instantaneous (elastic) response to seafloor loading = γ (referred to as the loading efficiency) (Fig. F18B) depends on porosity, Poisson's ratio, the compressibility of the solid grain constituents, the compressibility of the sediment or rock framework, and the compressibility of the interstitial fluid or fluid + gas mixture. With the first three of these being well known, absolute values and contrasts in observed loading efficiency can be used to constrain the effects of gas on the elastic properties of the fluid (and hence gas content) and the effect of gas hydrates on the elastic properties of the matrix (and hence average gas hydrate content).

In simple cases where a sharp mechanical properties contrast is present (e.g., at the seafloor or at the gas/gas hydrate boundary), a transient pressure gradient will be established and interstitial water will flow (Fig. **F18A**). A damped diffusional wave will propagate away from the boundary, adding a component to the signal (Fig. **F18B**) that decays with distance (Fig. **F18C**). At large distances, the response is purely elastic (γ) and constrains such things as the matrix compressibility, the gas content (Fig. **F18D**), and the coefficient that defines how tectonic deformation loads the interstitial water (Fig. **F18E**). At intermediate distances, the characteristic diffusion scale length, l (Fig. **F18C**), depends on the hydraulic diffusivity of the formation, η, and the period of the loading signal, P, as

$$l = (\pi\ \eta\ P)^{1/2}.$$

The broad bandwidth of ocean wave and tidal loading, for which periods range from seconds to weeks, combined with the distribution of the screens around the gas/gas hydrate boundary, should allow much to be learned about variations in formation elastic and hydrologic properties.

Operations summary

During Leg 146, two attempts were made to establish CORK hydrologic observatories, one at Site 889 and the other in a similar setting at ODP Site 892 off central Oregon (Westbrook, Carson, Musgrave, et al., 1994; Davis et al., 1995). These were equipped with sensors to monitor temperatures at multiple formation levels and pressure at the level of perforations in a liner extending below casing. The installation in Hole 892B was successful and operational for roughly 2 y before the instrumentation was removed to facilitate fluid sampling. Owing to unstable formation conditions and deteriorating weather, the installation in Hole 889C did not succeed. Instability of the formation caused sediment to be squeezed into the casing through the perforations, the open end of the liner, and/or the annulus between the liner and the casing. This prevented the thermistor cable from reaching its intended depth, which in turn precluded a pressure-tight seal of the pressure logging system at the top of the hole. The total hole depth was 385 mbsf; the bottom of the liner was at 323 mbsf. After two aborted attempts to deploy the thermistor cable, a sinker-bar run indicated fill had reached 253 mbsf. The failed third attempt with a cable shortened to 240 m suggested that sediment had progressively intruded the casing up to this depth. The CORK was never refurbished.

Expedition 328 began at 0836 h on 5 September 2010 when the first line was passed ashore at Ogden Point Pier A in Victoria, British Columbia (Canada). After completing port call public relations, logistical, and maintenance activities, we departed Victoria for Site U1364 (CAS-01CORK) when the last line was released at 1606 h on 9 September. After maneuvering away from the pier, the vessel began the 145 nmi transit to the site at 1700 h. The ship arrived on location (48°41.9962′N, 126°52.3291′W) at 0600 h on 10 September, concluding a transit that averaged 11.2 kt.

Our first objective was to perform a jet-in test to verify the water depth and establish the conductor casing length to be deployed with the reentry cone, followed by jetting the casing and reentry cone (Fig. **F19**). The vibration-isolated television (VIT) frame was deployed to observe the bit contacting the seafloor at 1329.0 meters below rig floor (mbrf), and the jet-in test was completed to 55 mbsf. Based on this result, the conductor casing was assembled consisting of three joints of 16 inch casing and a casing shoe joint for a total length of 53 m, which was latched into a standard reentry cone. Once the drilling BHA equipped with a 11⅞ inch advanced piston corer (APC)/extended core barrel (XCB) bit was latched into the casing hanger, the reentry cone was deployed, and the jetting of the reentry cone and casing was initiated at 0600 h on 12 September while being monitored via the VIT. The 53 m assembly was jetted in and landed by1435 h, and the drill string was tripped back to the rig floor.

The next operation was to drill a 14¾ inch hole to accommodate the 10¾ inch casing string (Fig. **F19**). A drilling BHA with a 14¾ drilling bit was made up and deployed, reentering Hole U1364A at 0905 h on 13 September. The VIT was recovered, and drilling advanced without incident to a final depth of 336.0 mbsf. Penetration rate and weight on bit were fairly constant throughout the history of drilling below the ~100 m thick unit of slope basin sediments, although a drop in weight on bit and a significant increase in penetration rate were observed over a ~20 m interval below the limit of gas hydrate stability (Fig. **F20**). High-viscosity mud sweeps (20 bbl each) were circulated at 164, 193, 222, 278, 307, and 336.0 mbsf. A large high-viscosity 50 bbl flush was pumped at the conclusion of drilling. The hole was then displaced with 250 bbl of 10.5 ppg barite-loaded mud. The drill string was recovered with the bit clearing the rotary table at 1435 h on 14 September.

The next step was to make up the ACORK assembly. The construction of the ACORK, which includes making connections to the hardware, strapping and taping the umbilical to the casing, and making the plumbing connections to the screens and ACORK, began at 1430 h on 14 September and continued to 1000 h on 15 September.

The ACORK assembly included a custom ACORK head, a 10¾ inch casing hanger, 20 joints of 10¾ inch casing, two pup joints of 10¾ inch casing, a TAM Freecap 10 inch × 14 inch dual-element swellable packer, and four screen joints of 10¾ inch casing and one shoe joint. The length of the entire assembly was 329.1 m. Because 6.0 m of ACORK head extended above the hang-off point in the reentry cone, the effective depth of the assembly into the hole was 323.1 m. This left a 12.9 m rat hole between the bottom of the casing shoe and the bottom of the hole at 336.0 mbsf. The next phase of rigging up was to make up a reaming BHA, which included a 9⅞ inch tricone bit, a 9.5 inch HOC DTU950 underreamer, a 9.5 inch Ultra XL mud motor, and the cam-actuated drill-ahead (CADA) casing running tool. The total length of this BHA was 418.9 m. As the BHA was being assembled, it was lowered incrementally into the ACORK suspended in the moonpool until the CADA running tool landed into the ACORK at 1345 h on 15 September. The ACORK and reaming assembly were then lowered into the water with the ACORK head ~10 m beneath the surface for 5 min to purge any entrapped air. The four purge valves were then manually turned to the closed position, the ACORK and reaming BHA were deployed, and Hole U1364A was entered for the second time at 1930 h. The ACORK was gradually lowered into the open hole until it was successfully landed in the reentry cone at 0025 h on 16 September. The hole appeared to have remained open, possibly because of the presence of the 10.5 ppg mud that was pumped into the hole at the conclusion of the drilling process, so no circulation or underreaming was required. It is anticipated that the barite (specific gravity = 4.2; average grain size ~ 44 µm) contained in the mud probably settled out to fill the lower few tens of meters of the hole and annulus around the lower screen within days. The mud remaining in the remainder of the annulus would have had a density little different than seawater, and thus not impede hole collapse.

The ROV platform was tethered to the VIT frame and deployed at 0400 h on 16 September. The platform was successfully deployed when the mechanical release activated upon contacting the CADA top hat at 0515 h. The VIT frame was then recovered.

A Hammer Drilling System (HDS) cone, adapted to fit over the 16 inch casing hanger at the top of the ACORK to facilitate reentry, was made up and free-fall deployed at 0820 h on 16 September. However, the cone was dislodged while retrieving the drill string and fell to the seafloor. The drilling string was tripped back to the rig floor.

The final operation was the deployment of a hydraulic packer to seal the bottom of the 10¾ inch casing. The packer assembly was deployed, and Hole U1364A was reen-

tered for the third time at 2320 h on 16 September. Although the 23¾ inch diameter throat of the ACORK presented a smaller target than the HDS cone, the reentry was made in <1 h. The packer was positioned at 319 mbsf or 4 m above the casing shoe with a circulating head in place. Prior to activating the packer, the inside of the casing was displaced with one volume of seawater while maintaining pressure below 200 psi to ensure that the packer would not inflate prematurely. At 0230 h, the activating steel ball was dropped into the pipe and seated inside the bridge plug. The pressure was gradually increased until the packer set at ~1300–1400 psi. The packer was released at 0335 h when ~2700 psi was applied. The driller pulled back in the hole, circulated seawater while waiting for the cement to be mixed, and then pumped ~4 bbl of 16 ppg cement, covering the packer with ~14 m of cement. The inside of the casing was then flushed with three volumes of seawater. At 0600 h, the driller began to recover the drill string, which was back onboard at 1400 h, ending operations at Site U1364.

The ship was secured for transit, the thrusters raised, and the ship departed for port. The *JOIDES Resolution* arrived at Esquimalt Graving Dock in Victoria at 0804 h on 18 September 2010, concluding Expedition 328.

References

Becker, K., Bartetzko, A., and Davis, E.E., 2001. Leg 174B synopsis: revisiting Hole 395A for logging and long-term monitoring of off-axis hydrothermal processes in young oceanic crust. *In* Becker, K., and Malone, M.J. (Eds.), *Proc. ODP, Sci. Results,* 174B: College Station, TX (Ocean Drilling Program), 1–12. **doi:10.2973/odp.proc.sr.174B.130.2001**

Becker, K., and Davis, E.E., 2005. A review of CORK designs and operations during the Ocean Drilling Program. *In* Fisher, A.T., Urabe, T., Klaus, A., and the Expedition 301 Scientists, *Proc. IODP,* 301: College Station, TX (Integrated Ocean Drilling Program Management International, Inc.). **doi:10.2204/iodp.proc.301.104.2005**

Becker, K., Fisher, A.T., and Davis, E.E., 1997. The CORK experiment in Hole 949C: long-term observations of pressure and temperature in the Barbados accretionary prism. *In* Shipley, T.H., Ogawa, Y., Blum, P., and Bahr, J.M. (Eds.), *Proc. ODP, Sci. Results,* 156: College Station, TX (Ocean Drilling Program), 247–252. **doi:10.2973/odp.proc.sr.156.031.1997**

Davis, E., and Becker, K., 1998. Borehole observatories record driving forces for hydrothermal circulation in young oceanic crust. *Eos, Trans. Am. Geophys. Union,* 79:369, 377–378. **doi:10.1029/98EO00275**

Davis, E., and Becker, K., 2007. On the fidelity of "CORK" borehole hydrologic observatory pressure records. *Sci. Drill.,* 5:54–59. **doi:10.2204/iodp.sd.5.09.2007**

Davis, E., Becker, K., Wang, K., and Kinoshita, M., 2009. Co-seismic and post-seismic pore-fluid pressure changes in the Philippine Sea plate and Nankai decollement in response to a seismogenic strain event off Kii Peninsula, Japan. *Earth, Planets Space,* 61:649–657.

Davis, E.E., and Becker, K., 1994. Formation temperatures and pressures in a sedimented rift hydrothermal system: 10 months of CORK observations, Holes 857D and 858G. *In* Mottl, M.J., Davis, E.E., Fisher, A.T., and Slack, J.F. (Eds.), *Proc. ODP, Sci. Results,* 139: College Station, TX (Ocean Drilling Program), 649–666. **doi:10.2973/odp.proc.sr.139.255.1994**

Davis, E.E., and Becker, K., 1999. Tidal pumping of fluids within and from the oceanic crust: new observations and opportunities for sampling the crustal hydrosphere. *Earth Planet. Sci. Lett.,* 172(1–2):141–149. **doi:10.1016/S0012-821X(99)00197-1**

Davis, E.E., Becker, K., Pettigrew, T., Carson, B., and MacDonald, R., 1992. CORK: a hydrologic seal and downhole observatory for deep-ocean boreholes. *In* Davis, E.E., Mottl, M.J., Fisher, A.T., et al., *Proc. ODP, Init. Repts.,* 139: College Station, TX (Ocean Driling Program), 43–53. **doi:10.2973/odp.proc.ir.139.103.1992**

Davis, E.E., Becker, K., Wang, K., and Carson, B., 1995. Long-term observations of pressure and temperature in Hole 892B, Cascadia accretionary prism. *In* Carson, B., Westbrook, G.K., Musgrave, R.J., and Suess, E. (Eds.), *Proc. ODP, Sci. Results,* 146 (Pt. 1): College Station, TX (Ocean Drilling Program), 299–311. **doi:10.2973/odp.proc.sr.146-1.219.1995**

Davis, E.E., Hyndman, R.D., and Villinger, H., 1990. Rates of fluid expulsion across the northern Cascadia accretionary prism: constraints from new heat flow and multichannel seismic reflection data. *J. Geophys. Res.,* 95:8869–8889.

Davis, E.E., and Villinger, H.W., 2006. Transient formation fluid pressures and temperatures in the Costa Rica forearc prism and subducting oceanic basement: CORK monitoring at ODP Sites 1253 and 1255. *Earth Planet. Sci. Lett.,* 245(1–2):232–244. **doi:10.1016/j.epsl.2006.02.042**

Davis, E.E., Wang, K., Becker, K., and Thomson, R.E., 2000. Formation-scale hydraulic and mechanical properties of oceanic crust inferred from pore pressure response to periodic

seafloor loading. *J. Geophys. Res., [Solid Earth],* 105(B6):13423–13436. **doi:10.1029/2000JB900084**

Davis, E.E., Wang, W., Thomson, R.E., Becker, K., and Cassidy, J.F., 2001. An episode of seafloor spreading and associated plate deformation inferred from crustal fluid pressure transients. *J. Geophys. Res., [Solid Earth],* 106(B10):21953–21963. **doi:10.1029/2000JB000040**

DeMets, C., Gordon, R.G., Argus, D.F., and Stein, S., 1990. Current plate motions. *Geophys. J. Int.,* 101(2):425–478. **doi:10.1111/j.1365-246X.1990.tb06579.x**

Fisher, A.T., Wheat, C.G., Becker, K., Davis, E.E., Jannasch, H., Schroeder, D., Dixon, R., Pettigrew, T.L., Meldrum, R., McDonald, R., Nielsen, M., Fisk, M., Cowen, J., Bach, W., and Edwards, K., 2005. Scientific and technical design and deployment of long-term subseafloor observatories for hydrogeologic and related experiments, IODP Expedition 301, eastern flank of Juan de Fuca Ridge. *In* Fisher, A.T., Urabe, T., Klaus, A., and the Expedition 301 Scientists, *Proc. IODP,* 301: College Station, TX (Integrated Ocean Drilling Program Management International, Inc.). **doi:10.2204/iodp.proc.301.103.2005**

Foucher, J.-P., Henry, P., and Harmegnies, F., 1997. Long-term observations of pressure and temperature in Hole 948D, Barbados accretionary prism. *In* Shipley, T.H., Ogawa, Y., Blum, P., and Bahr, J.M. (Eds.), *Proc. ODP, Sci. Results,* 156: College Station, TX (Ocean Drilling Program), 239–245. **doi:10.2973/odp.proc.sr.156.045.1997**

Goldfinger, C., Nelson, C.H., Johnson, J.E., and the Shipboard Scientific Party, 2003. Holocene earthquake records from the Cascadia subduction zone and northern San Andreas fault based on precise dating of offshore turbidites. *Annu. Rev. Earth Planet. Sci.,* 31(1):555–577. **doi:10.1146/annurev.earth.31.100901.141246**

Haacke, R.R., Westbrook, G.K., and Hyndman, R.D., 2007. Gas hydrate, fluid flow and free gas: formation of the bottom-simulating reflector. *Earth Planet. Sci. Lett.,* 261(3–4):407–420. **doi:10.1016/j.epsl.2007.07.008**

Hyndman, R.D., and Davis, E.E., 1992. A mechanism for the formation of methane hydrate and seafloor bottom-simulating reflectors by vertical fluid expulsion. *J. Geophys. Res., [Solid Earth],* 97(B5):7025–7041. **doi:10.1029/91JB03061**

Jannasch, H.W., Davis, E.E., Kastner, M., Morris, J.D., Pettigrew, T.L., Plant, J.N., Solomon, E.A., Villinger, H.W., and Wheat, C.G., 2003. CORK-II: long-term monitoring of fluid chemistry, fluxes, and hydrology in instrumented boreholes at the Costa Rica subduction zone. *In* Morris, J.D., Villinger, H.W., Klaus, A., *Proc. ODP, Init. Repts.,* 205: College Station, TX (Ocean Drilling Program), 1–36. **doi:10.2973/odp.proc.ir.205.102.2003**

Kao, H., Shan, S.-J., Dragert, H., Rogers, G., Cassidy, J.F., Wang, K., James, T.S., and Ramachandran, K., 2006. Spatial-temporal patterns of seismic tremors in northern Cascadia. *J. Geophys. Res., [Solid Earth],* 111(B3):B03309. **doi:10.1029/2005JB003727**

Kastner, M., Becker, K., Davis, E.E., Fisher, A.T., Jannasch, H.W., Solomon, E.A., and Wheat, G., 2006. New insights into the hydrogeology of the oceanic crust through long-term monitoring. *Oceanography,* 19(4):46–57. **http://www.tos.org/oceanography/issues/issue_archive/issue_pdfs/19_4/19.4_kastner_et_al.pdf**

Leonard, L.J., Currie, C.A., Mazzotti, S., and Hyndman, R.D., 2010. Rupture area and displacement of past Cascadia great earthquakes from coastal coseismic subsidence. *Geol. Soc. Am. Bull.* **doi:10.1130/B30108.1**

Mikada, H., Becker, K., Moore, J.C., Klaus, A., et al., 2002. *Proc. ODP, Init. Repts.,* 196: College Station, TX (Ocean Drilling Program). **doi:10.2973/odp.proc.ir.196.2002**

Riedel, M., 2001. 3D seismic investigations of northern Cascadia marine gas hydrates [Ph.D. dissert.]. Univ. Victoria, Canada.

Riedel, M., Collett, T.S., and Malone, M., 2010. Expedition 311 synthesis: scientific findings. *In* Riedel, M., Collett, T.S., Malone, M.J., and the Expedition 311 Scientists, *Proc. IODP,* 311: Washington, DC (Integrated Ocean Driling Program Management International, Inc.). **doi:10.2204/iodp.proc.311.213.2010**

Riedel, M., Collett, T.S., Malone, M.J., and the Expedition 311 Scientists, 2006. *Proc. IODP,* 311: Washington, DC (Integrated Ocean Drilling Program Management International, Inc.). **doi:10.2204/iodp.proc.311.2006**

Riedel, M., Paull, C.K., Spence, G., Hyndman, R.D., Caress, D.W., Thomas, H., Lundsten, E., Ussler, W., and Schwalenberg, K., 2009. Geophysical signatures of cold vents on the northern Cascadia margin. *Eos, Trans. Am. Geophys. Union,* 90(52)(Suppl.):OS31A-1196. (Abstract) **http://www.agu.org/meetings/fm09/waisfm09.html**

Ryan, W.B.F., Carbotte, S.M., Coplan, J.O., O'Hara, S., Melkonian, A., Arko, R., Weissel, R.A., Ferrini, V., Goodwillie, A., Nitsche, F., Bonczkowski, J., and Zemsky, R., 2009. Global multi-resolution topography synthesis. *Geochem., Geophys., Geosyst.,* 10(3):Q03014. **doi:10.1029/2008GC002332**

Salisbury, M.H., Shinohara, M., Richter, C., et al., 2002. *Proc. ODP, Init. Repts.,* 195: College Station, TX (Ocean Drilling Program). **doi:10.2973/odp.proc.ir.195.2002**

Satake, K., Shimazaki, K., Tsuji, Y., and Ueda, K., 1996. Time and size of a giant earthquake in Cascadia inferred from Japanese tsunami records of January 1700. *Nature (London, U. K.),* 379(6562):246–249. **doi:10.1038/379246a0**

Scherwath, M., Riedel, M., Spence, G.D., and Hyndman, R.D., 2006. Data report: seismic structure beneath the north Cascadia drilling transect of IODP Expedition 311. *In* Riedel, M., Collett, T.S., Malone, M.J., and the Expedition 311 Scientists, *Proc. IODP,* 311: Washington, DC (Integrated Ocean Drilling Program Management International, Inc.). **doi:10.2204/iodp.proc.311.110.2006**

Screaton, E.J., Carson, B., and Lennon, G.P., 1995. Hydrogeologic properties of a thrust fault within the Oregon accretionary prism. *J. Geophys Res., [Solid Earth],* 100(B10):20025–20035. **doi:10.1029/95JB02152**

Screaton, E.J., Fisher, A.T., Carson, B., and Becker, K., 1997. Barbados Ridge hydrogeologic tests: implications for fluid migration along an active decollement. *Geology,* 25(3):239–242. **doi:10.1130/0091-7613(1997)025<0239:BRHTIF>2.3.CO;2**

Wang, K., and Davis, E.E., 1996. Theory for the propagation of tidally induced pore pressure variations in layered subseafloor formations. *J. Geophys. Res., [Solid Earth],* 101(B5):11483–11495. **doi:10.1029/96JB00641**

Wang, K., Davis, E.E., and van der Kamp, G., 1998. Theory for the effects of free gas in subsea formations on tidal pore pressure variations and seafloor displacements. *J. Geophys. Res., [Solid Earth],* 103(B6):12339–12354. **doi:10.1029/98JB00952**

Westbrook, G.K., Carson, B., Musgrave, R.J., et al., 1994. *Proc. ODP, Init. Repts.,* 146 (Pt. 1): College Station, TX (Ocean Drilling Program). **doi:10.2973/odp.proc.ir.146-1.1994**

Wheat, C.G., Fryer, P., Fisher, A.T., Hulme, S., Jannasch, H., Mottl, M.J., and Becker, K., 2008. Borehole observations of fluid flow from South Chamorro Seamount, an active serpentinite mud volcano in the Mariana forearc. *Earth Planet. Sci. Lett.,* 267(3–4):401–409. **doi:10.1016/j.epsl.2007.11.057**

Table T1. Electronic set-up of logging instrumentation of individual pressure sensors, Expedition 328. (**See table notes.**)

Sensor			Digitizer			AWQ
Target	Type	Serial number	Channel	Serial number	Version	Connector wedge*
Housing temperature	Platinum chip	92	RTC†	2010R08	8e	NA
Gauge temperature	Paroscientific Type II	119147	PPC9	2010R08	8cT	C2
Screen #1 pressure	Paroscientific Type I	119141	PPC1	2010S02	8c	C1
Screen #2 pressure	Paroscientific Type I	119144	PPC3	2010D04	8c	D1
Screen #3 pressure	Paroscientific Type I	119145	PPC4	2010D04	8c	F1
Screen #4 pressure	Paroscientific Type I	119146	PPC5	2010D05	8c	E1
Seafloor pressure	Paroscientific Type II	119147	PPC6	2010D05	8c	C2

Notes: * = there are two Seacon Inc. model AWQ "pie" connectors on the instrument pressure case with six connector wedges (A–F) each. Two are used for the RS-422 serial connection and external power, and five are used for connections to pressure sensors. † = the RTC (real time clock/controller) ID byte is 08. PPC = Precision period counter. NA = not applicable.

Table T2. Unparsed and parsed data format, Expedition 328.

Raw data
2AB61B04 08 83A839 2AD90E85 828E9D8D 811C3486 83885008 7EC23806 7ED377F700
2AB61B40 08 83A5DF 2AD90DB9 828E8E11 811C3122 8388438B 7EC2262D 7ED3677E00
2AB61B7C 08 83A2CE 2AD90CEF 828E9528 811C3440 838849CF 7EC22D76 7ED36EDD00

Calibrated data								
Date/Time	ID	T(plat)	T(sens)	P(Scr1)	P(Scr2)	P(Scr3)	P(Scr4)	P(Sf)
2010-09-15 17:19:00	08	14.6525	14.5444	11.6312	10.7216	11.4335	11.8392	11.9238
2010-09-15 17:20:00	08	14.6543	14.5452	11.6578	10.7277	11.4538	11.8704	11.9523
2010-09-15 17:21:00	08	14.6566	14.5461	11.6456	10.7229	11.4439	11.8582	11.9397

Table T3. Calibration coefficients of the deployed Paroscientific pressure gauges, Expedition 328.

Serial number:	119141	119144	119145	119146	119147
Measurement at:	Screen #1	Screen #2	Screen #3	Screen #4	Seafloor
U_0 (µs)	0	0	0	0	5.840718E+00
Y_1 (°C/µs)	0	0	0	0	–3.821929E+03
Y_2 (°C/µs^2)	0	0	0	0	–1.030901E+04
C_1 (psia)	–3.158282E+04	–3.033506E+04	–2.968242E+04	–3.143798E+04	–3.140634E+04
C_2 (psia/µs)	3.785890E–01	6.263960E–01	2.863060E–01	7.796390E–01	–2.346166E+03
C_3 (psia/µs^2)	8.336180E–03	1.159550E–02	1.073710E–02	1.065190E–02	9.194924E+04
D_1	3.980500E–02	4.043700E–02	3.988500E–02	3.888400E–02	3.833200E–02
T_1 (µs)	3.020867E+01	3.009071E+01	3.028336E+01	2.990774E+01	2.991600E+01
T_2 (µs/µs)	–1.104830E–04	1.922490E–04	1.121550E–05	1.784190E–04	7.295400E–02
T_3 (µs/µs^2)	3.611890E–06	4.415440E–06	4.254300E–06	3.997260E–06	5.473191E+01
T_4 (µs/µs^3)	3.793720E–09	1.858300E–09	2.918990E–09	2.932220E–09	1.361464E+02

Figure F1. Map showing regional context of Site U1364 (generated using GeoMapApp [www.geomapapp.org/] and the global multiresolution topography synthesis [Ryan et al., 2009]), including the NEPTUNE cable route and other boreholes in the area. With the exception of ODP Site 888, holes at all sites are sealed and instrumented with CORK observatories. ODP Hole 1026B is currently connected to the NEPTUNE cable.

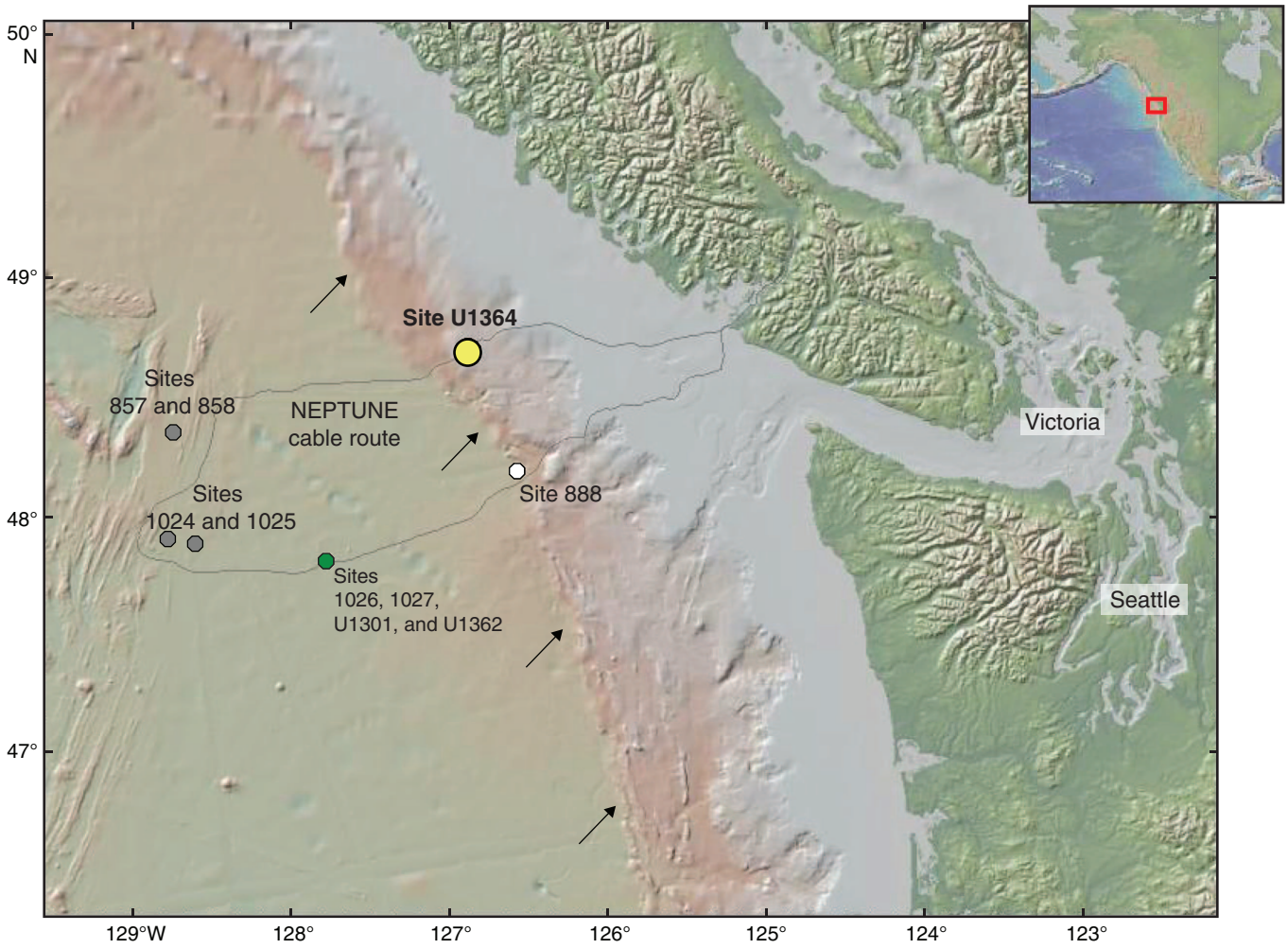

Figure F2. Multichannel seismic profile crossing the Cascadia accretionary prism and Site U1364 (location given in Fig. F3). BSR = bottom-simulating reflector.

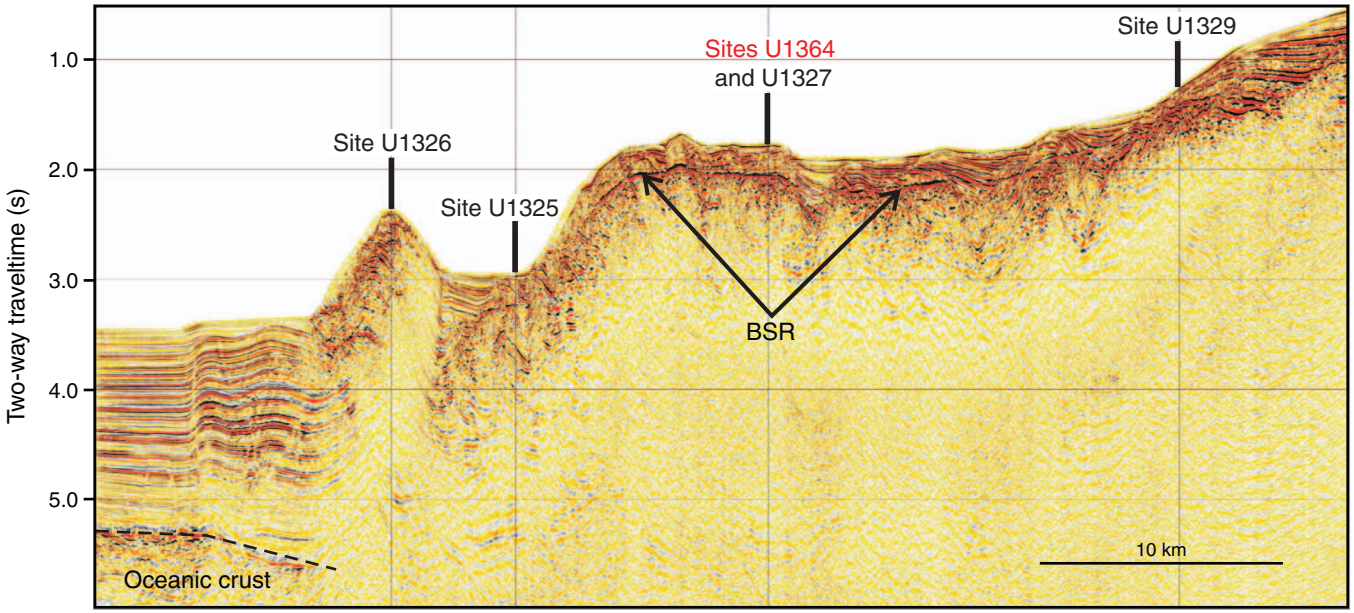

Figure F3. Seafloor morphology of the outer Cascadia accretionary prism in the vicinity of Site U1364. Locations of the drilling site, the seismic line in Figure F2, and the NEPTUNE cable route are indicated.

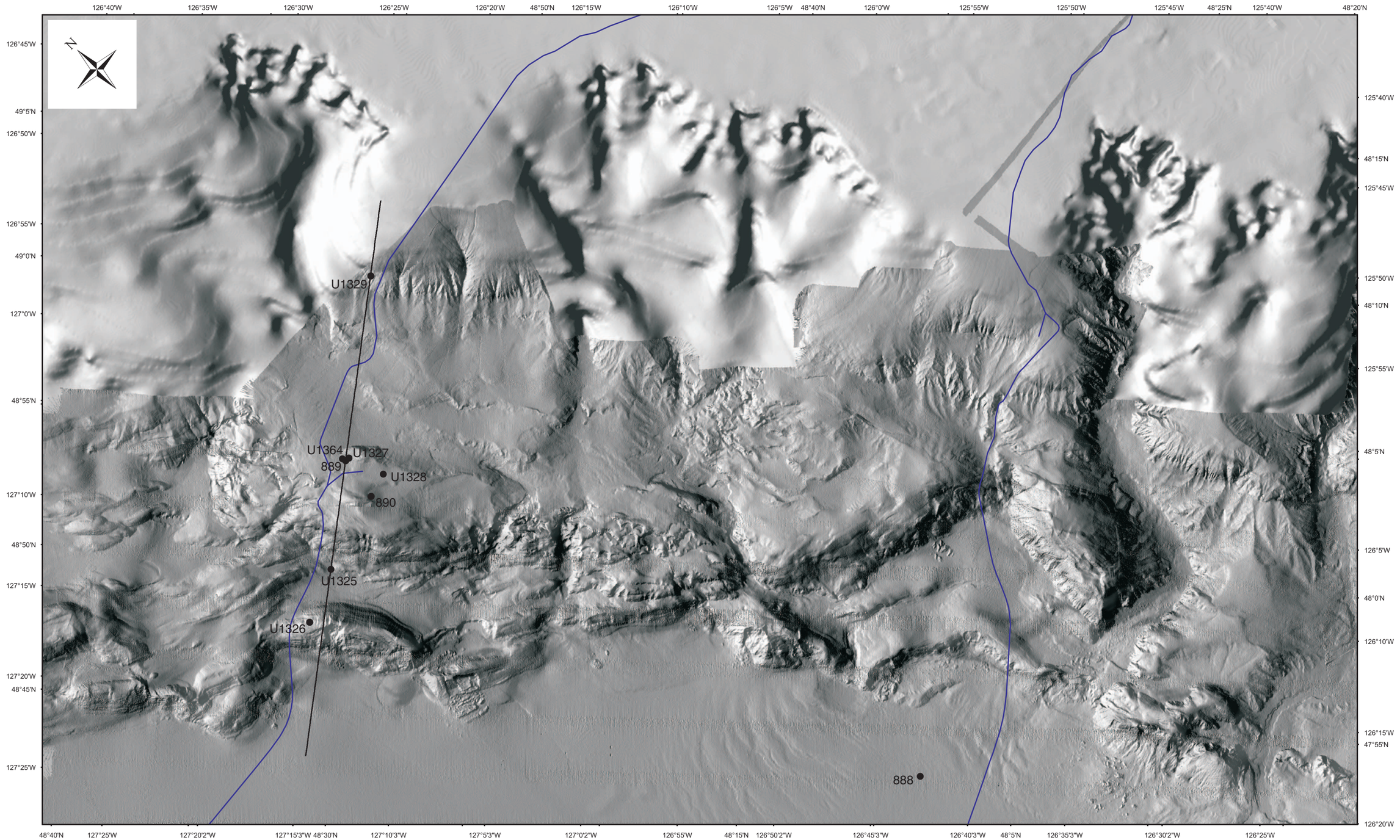

Figure F4. Detailed morphology of the seafloor in the immediate vicinity of Site U1364, including the location of formation-water and gas seeps (open triangles; Riedel et al., 2009) and boreholes drilled during Leg 146 and Expedition 311.

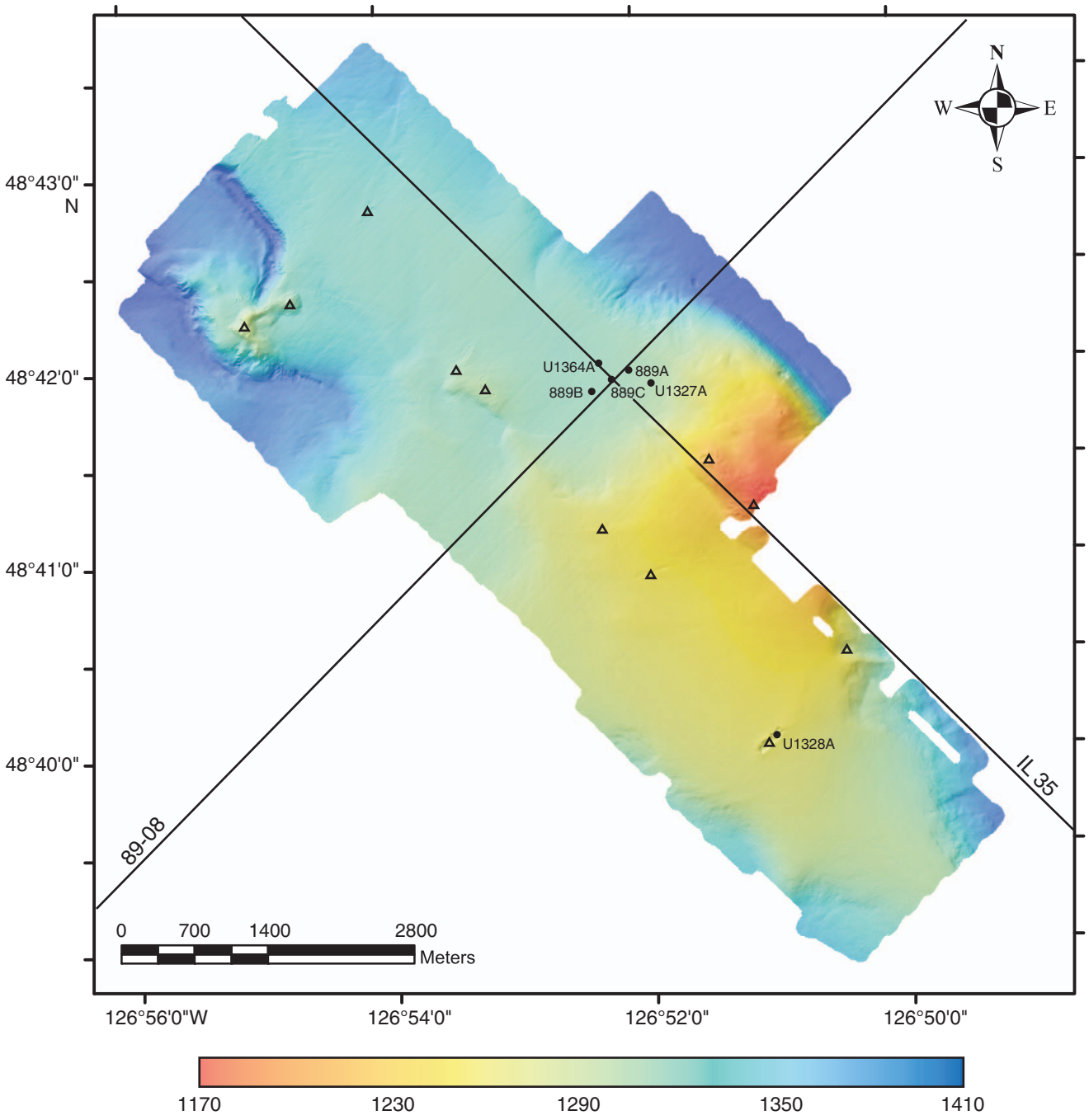

Figure F5. Schematic illustration of the first-order processes thought to be important in the formation of gas hydrates and associated bottom-simulating reflectors in subduction zone accretionary prisms (after Hyndman and Davis, 1992, and Riedel et al., 2010).

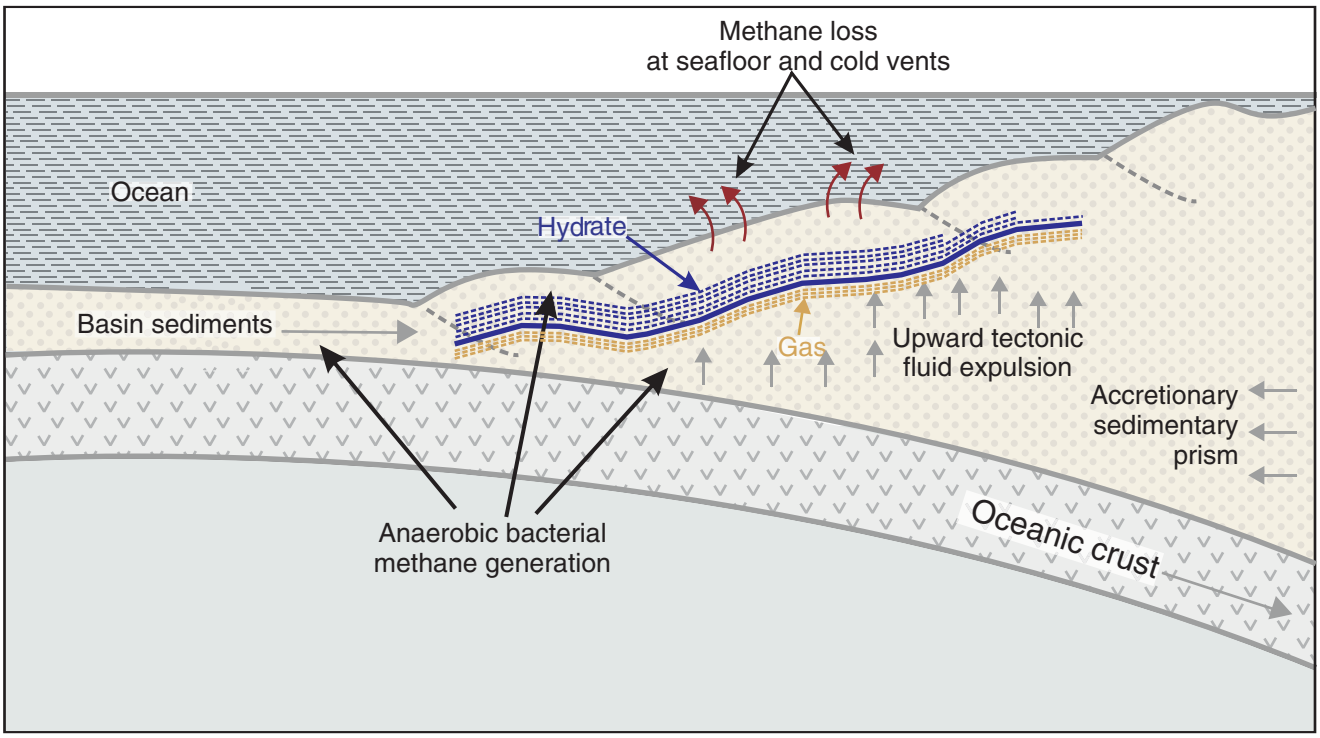

Figure F6. Seismic reflection profiles crossing Site U1364 and other boreholes nearby. Clearly visible are the gas hydrate bottom-simulating reflector (BSR) and the contact between deformed accretionary prism sediments and overlying slope basing deposits that are characterized by coherent seismic reflectors. **A.** Strike line, done with a large air gun array source. (**Continued on next page.**)

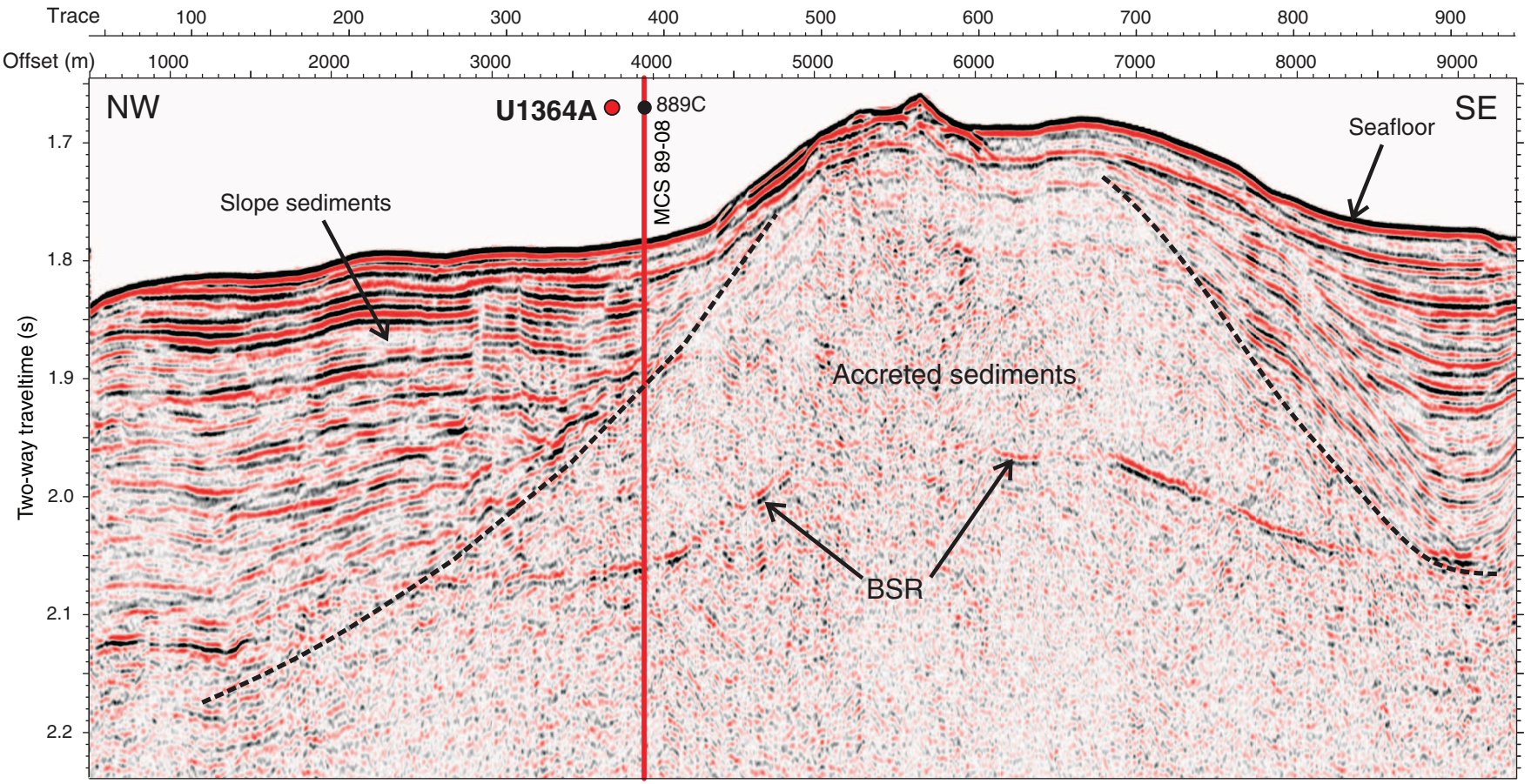

Figure F6 (continued). B. Dip line, done with a water-gun source, providing less penetration but greater resolution.

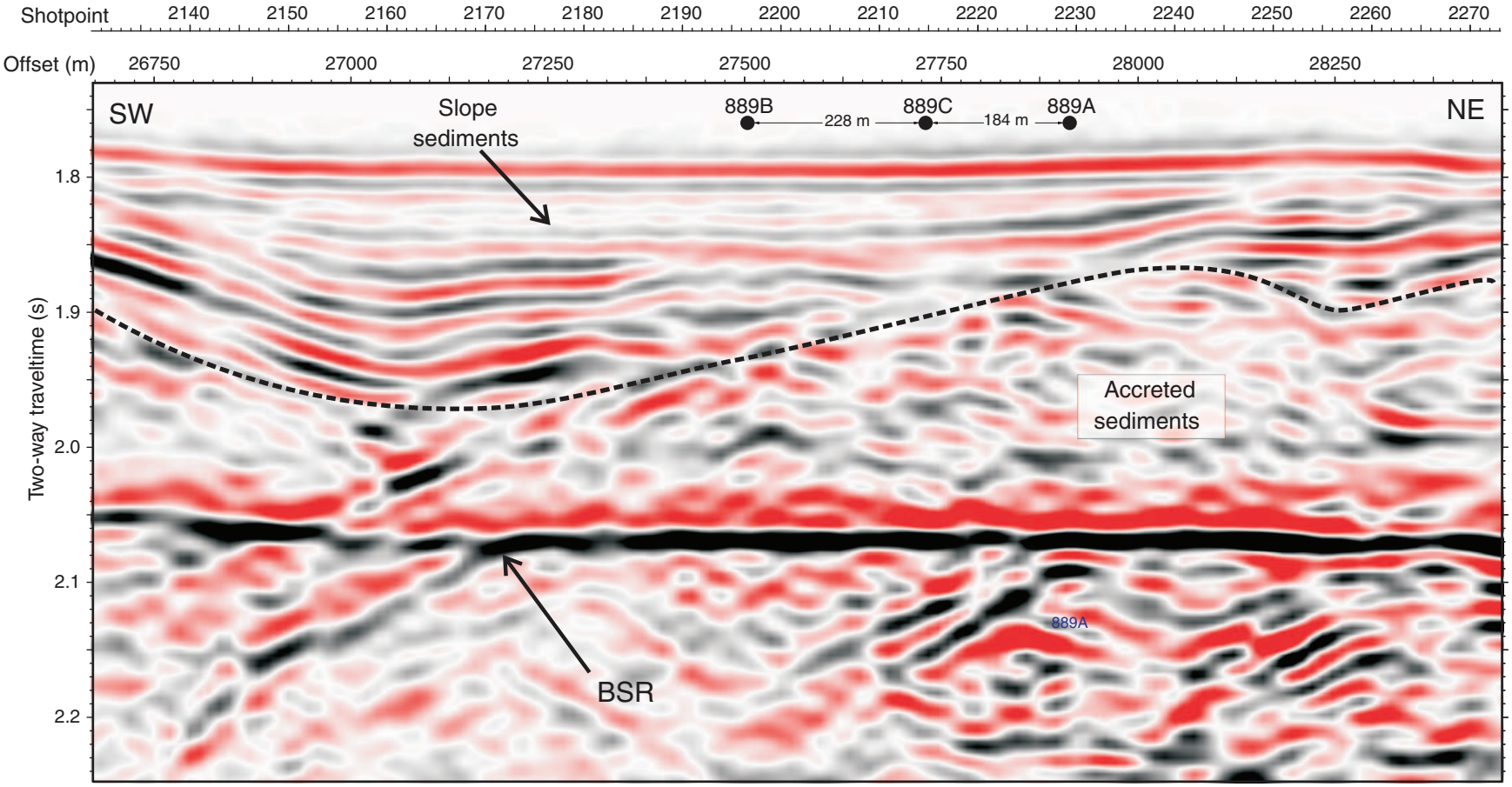

Figure F7. Logging data from Site U1327 (Riedel, Collett, Malone, et al., 2006), with the depths of the Site U1364 ACORK screens superimposed. Black traces are LWD logs from Hole U1327A; gray traces are wireline logs from Holes U1327D and U1327E <50 m away. Hole U1364A lies ~500 m to the northwest (see Fig. **F4** for locations). RAB = resistivity-at-the-bit.

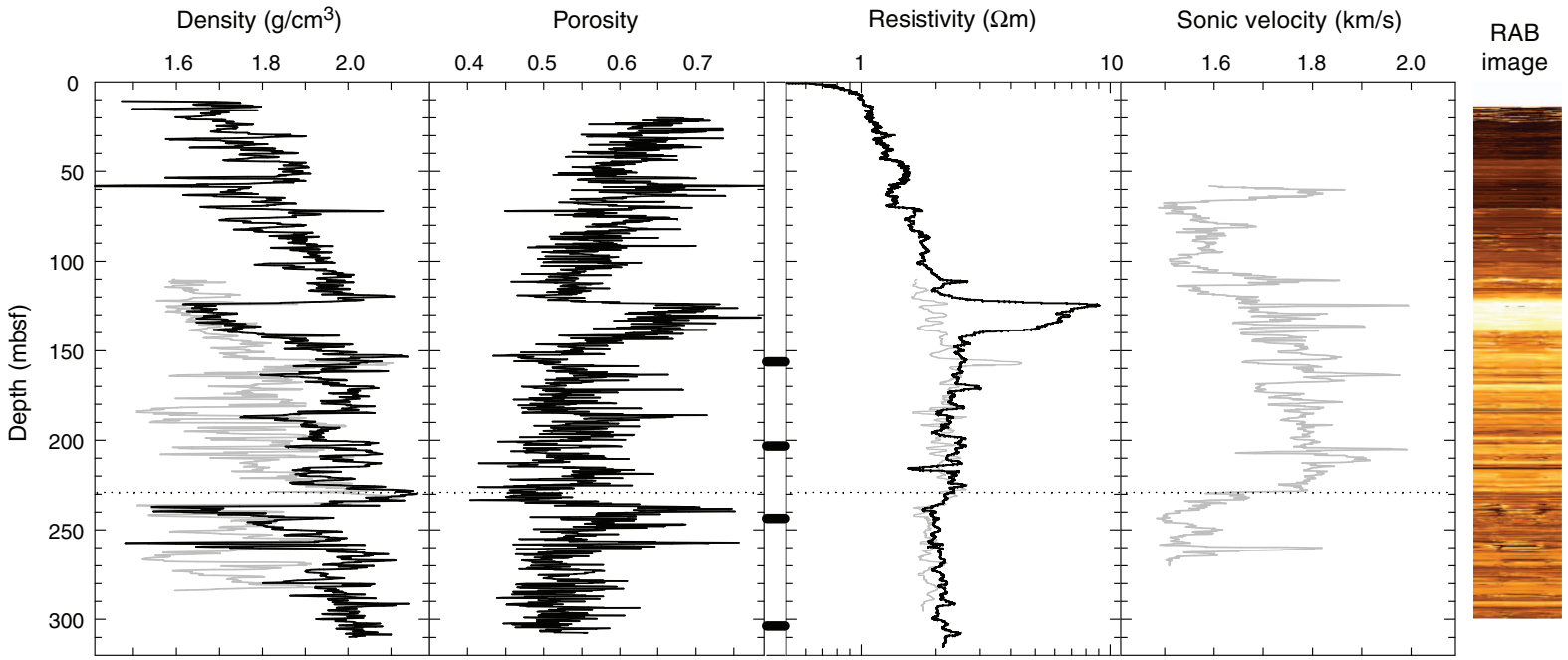

Figure F8. Pressure record from ODP Hole 1255A at the toe of the Costa Rica subduction zone prism, showing secular change possibly associated with interseismic strain accumulation and transients associated with small aseismic slip events on the subduction thrust (from Davis et al., submitted).

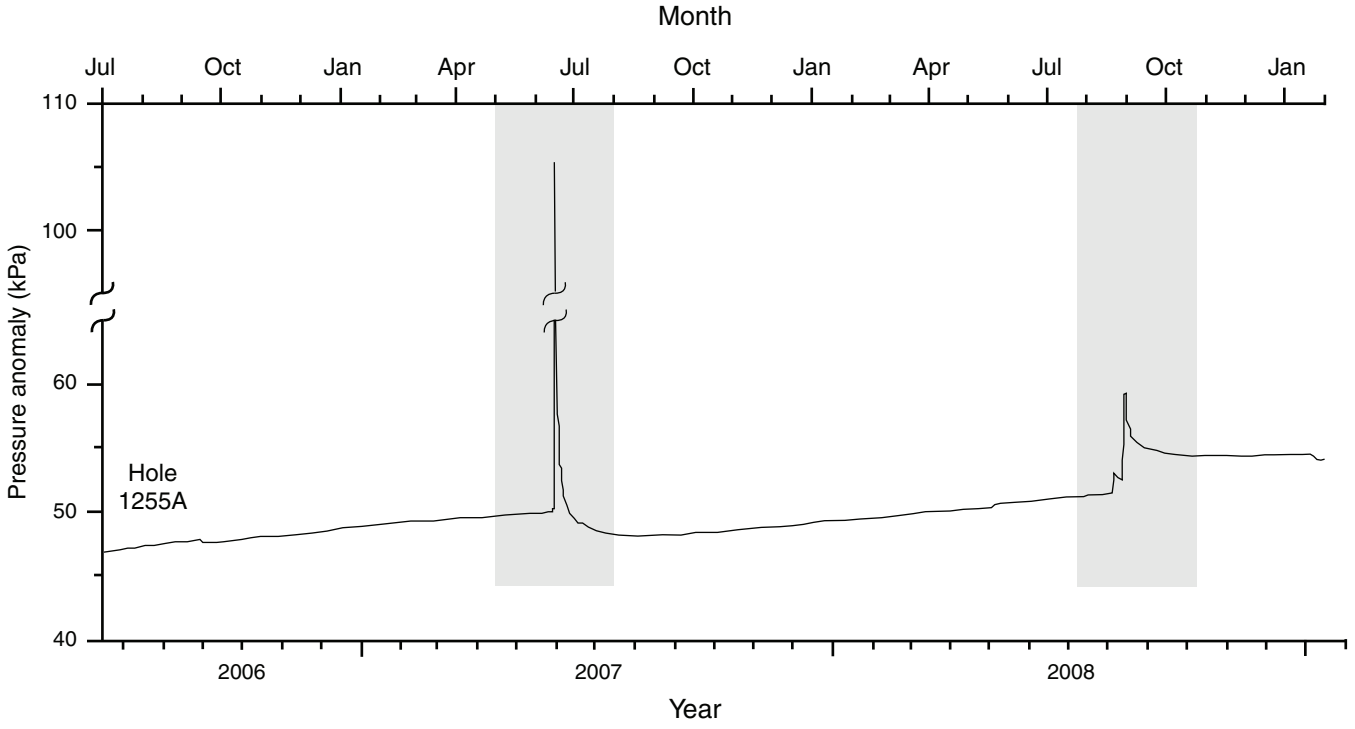

Figure F9. Seismicity in the northern Cascadia region. **A.** Epicenters of earthquakes in the oceanic crust shown as black open circles and in the continental crust as blue open circles (undifferentiated by magnitude). Large historical continental earthquakes (Mw ~7) are shown by red stars. **B.** Epicenters of tremor associated with periodic slip occurring roughly every 14 months documented along and above the subduction plate interface, shown as red open circles (from Kao et al., 2009). ETS = episodic tremor and slip.

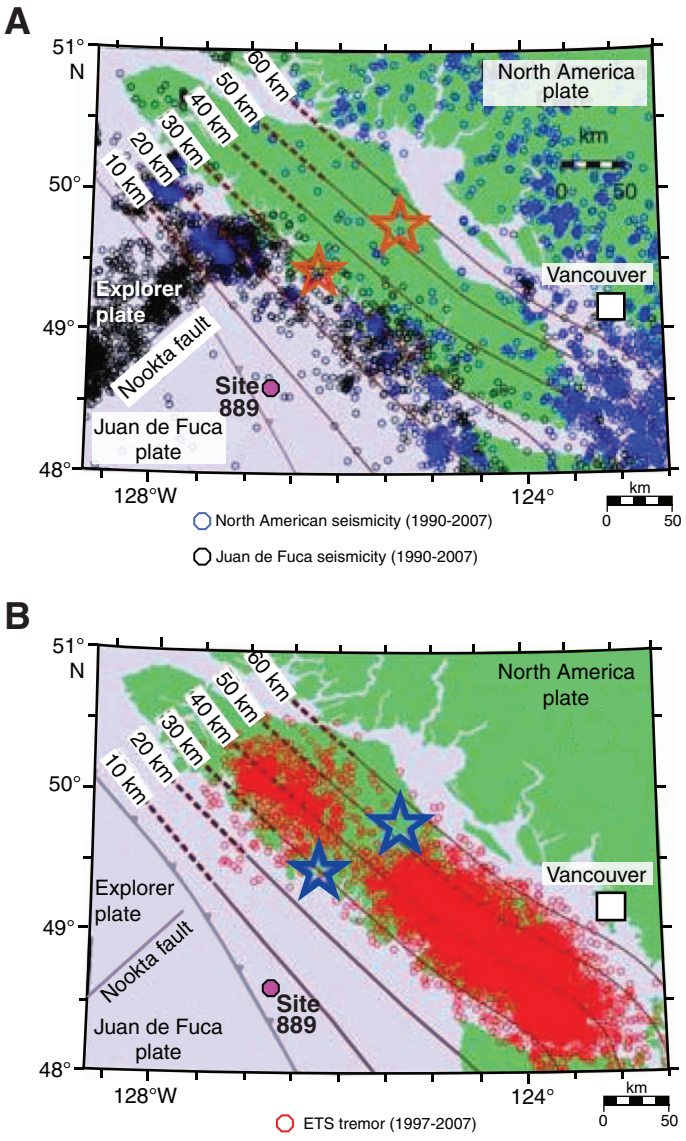

Figure F10. Pressure transients observed at CORKed ODP Hole 1027C revealing strain associated with seismogenic slip at the time of two regional earthquakes in 1996 and 1999 (Mw = 6.3 and 4.6, respectively). The sense of strain (expansional in 1996, contractional in 1999) is in each case consistent with that predicted on the basis of the earthquake moment tensors. The CORK observatory in this hole is completed in highly permeable oceanic crust; lateral fluid flow beneath the extensive low permeability sediment cover causes eventual drainage of the anomalous pressure. Transients associated with these events were observed at the other CORKed boreholes in the area as well (Davis et al., 2001; Kastner et al., 2006).

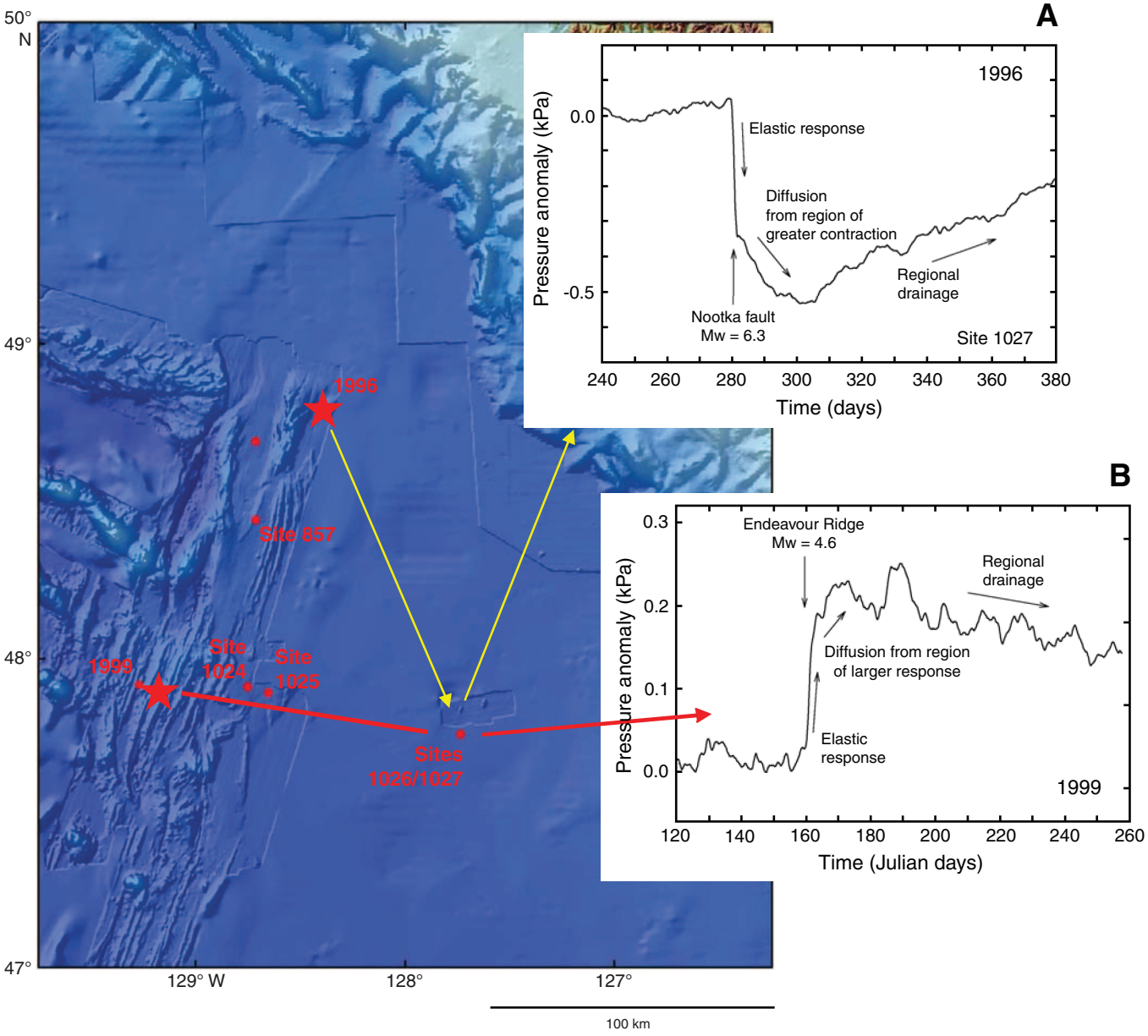

Figure F11. Recurrence statistics for earthquakes within 150 km of Site U1364. With the threshold experienced with CORK observatories to date, we expect resolvable seismic and strain signals like those shown in Figures F10 and F12 roughly once per year.

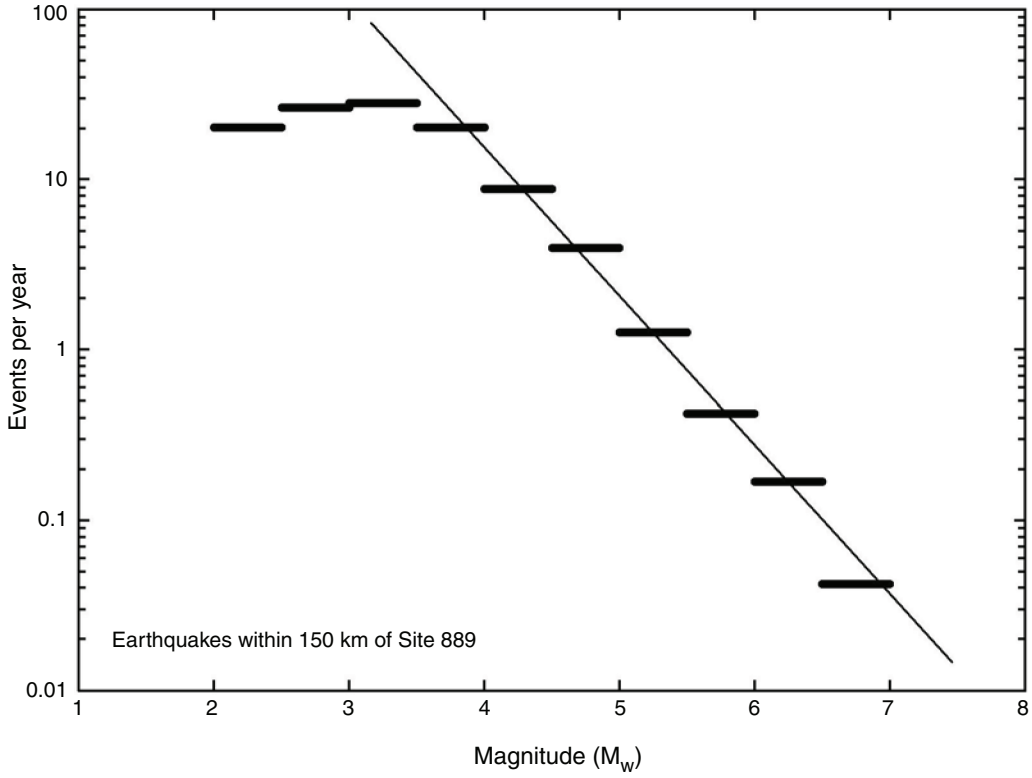

Figure F12. CORK pressure record of seismic surface waves and the tsunami generated by the 2010 Chile subduction zone earthquake. (**A**) Raw pressure records are dominated by tides, which are removed to reveal (**B**) seismic surface waves and (**C**) the following tsunami. BPR = bottom pressure recorder.

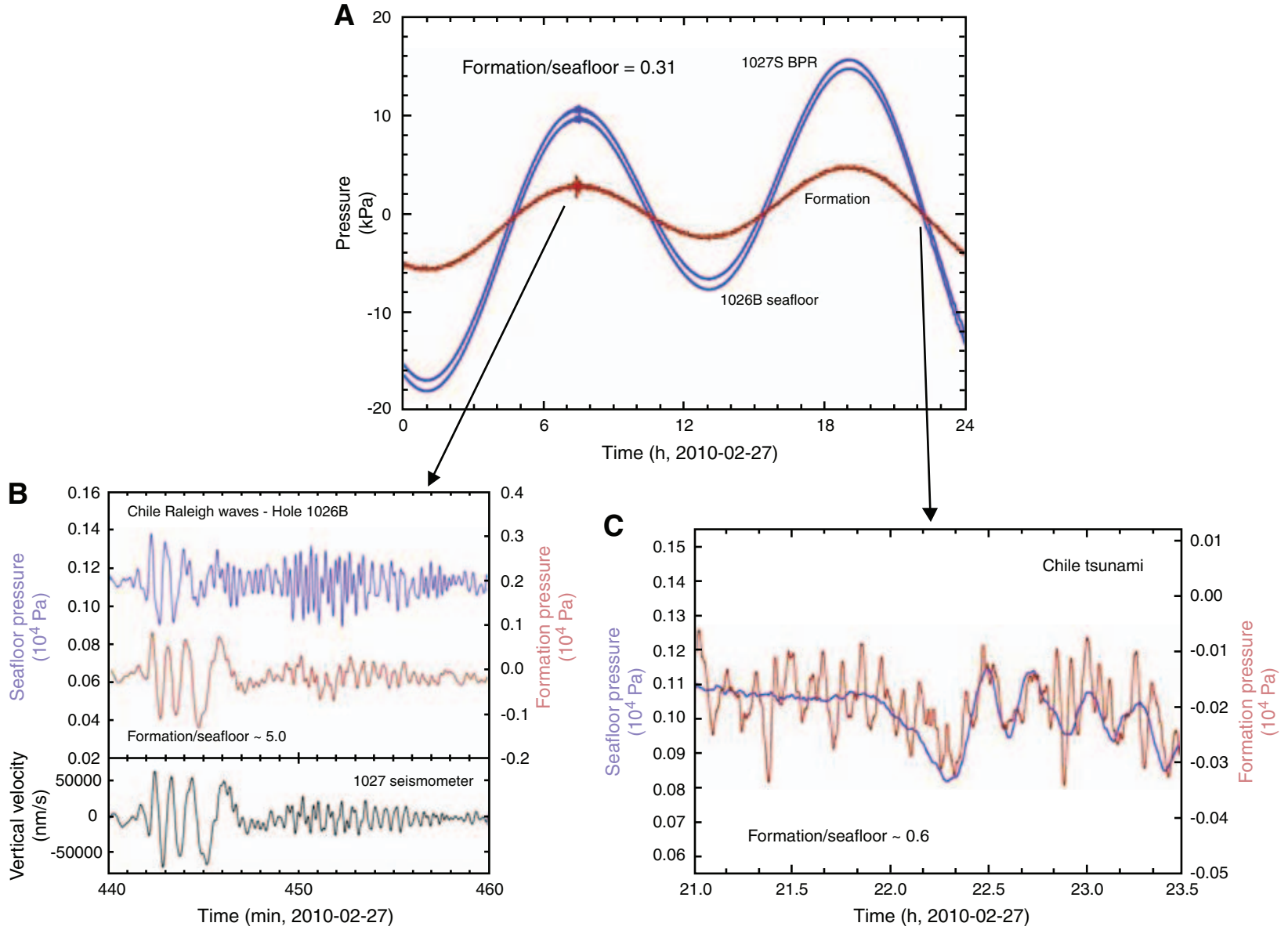

Figure F13. Wire-wrapped screens on solid 10¾ inch casing used during Expedition 328 to transmit formation pressures to the ACORK sensors via the umbilical cable shown in Figure **F14.** One hydraulic line in each screen is perforated for pressure signal transmission within the screen; the others pass through to transmit signals up to the wellhead from screens below (see Fig. **F19**). (Photo credit: Mary Reagan.)

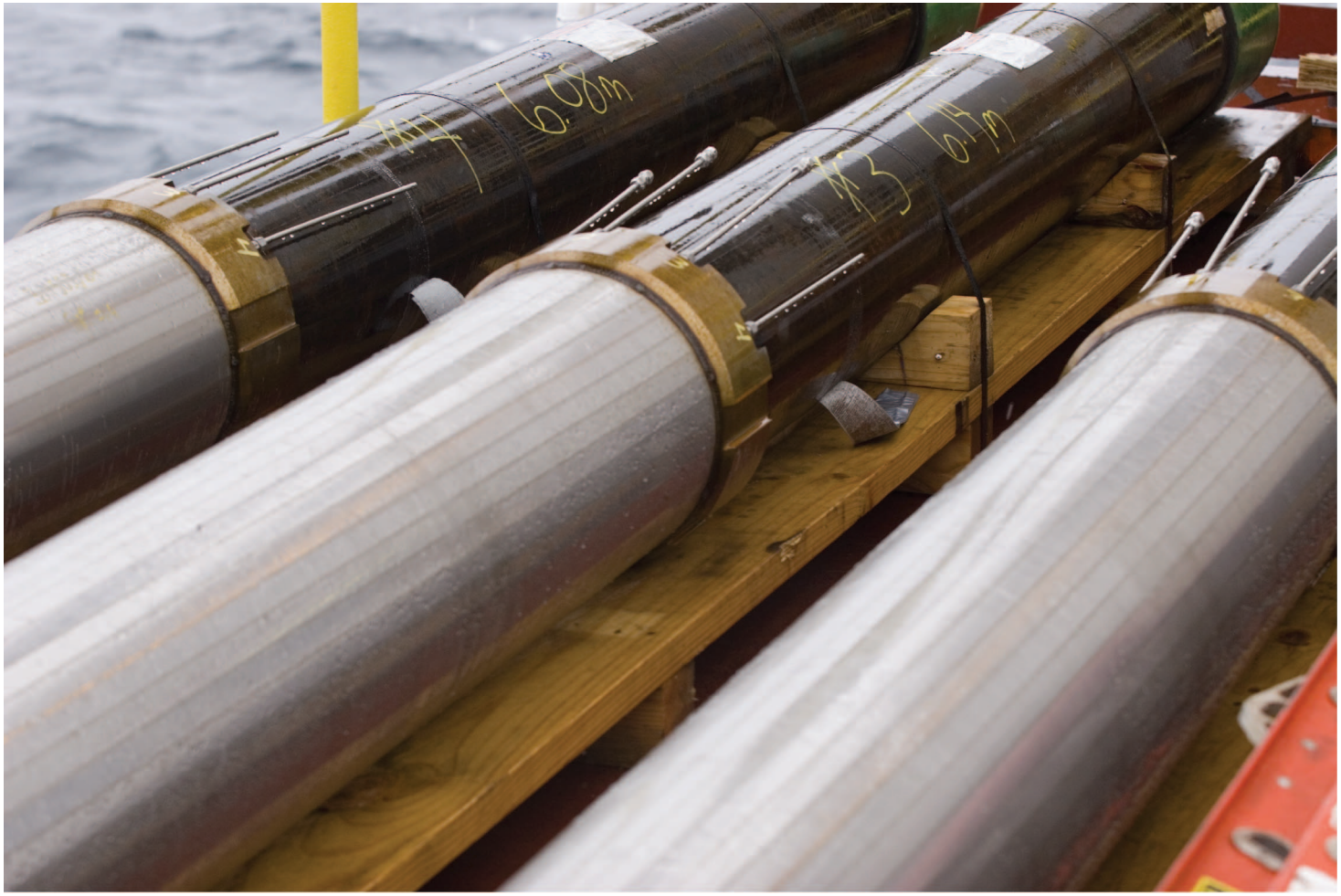

Figure F14. Polyurethane-jacketed umbilical used during Expedition 328 containing four stainless steel hydraulic tubes for pressure signal transmission from formation screens (Fig. **F13**) to wellhead sensors (Fig. **F16**).

Figure F15. Photos of ACORK seafloor structure used for Hole U1364A. (Photo credit: Martin Heesemann.) **A.** The instrument bay. (**Continued on next page.**)

Figure F15 (continued). B. Detailed view of the casing hanger used for hanging the system when it is drilled in for reentry with the drill string to seal the bottom of the 10¾ inch casing with a bridge plug and cement and later for wireline installation of instruments.

Figure F16. ACORK pressure monitoring instrument. **A.** Components photos. AWQ = pressure case bulkhead connectors. (Photo credit: Martin Heesemann.) (**Continued on next five pages.**)

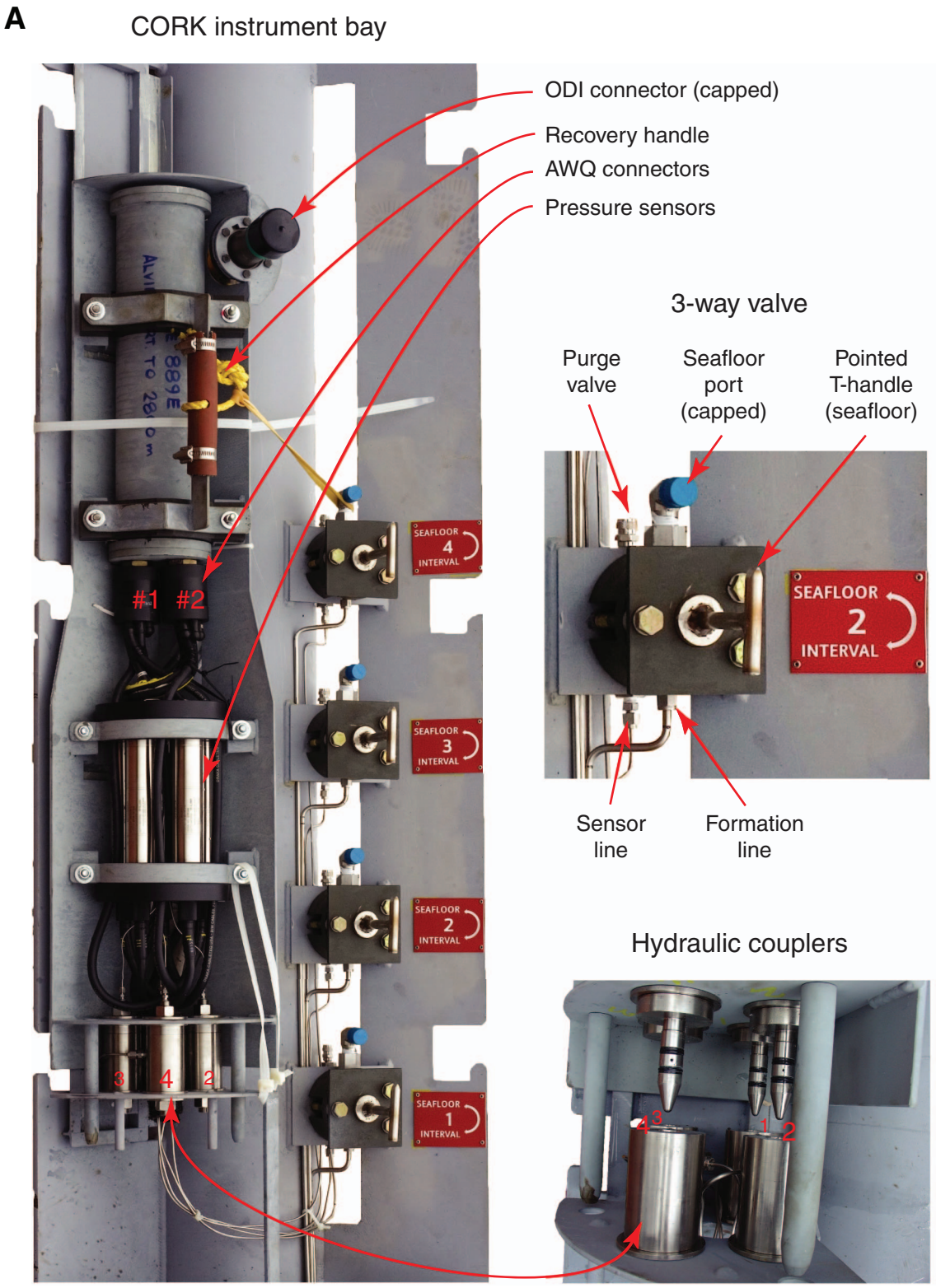

Figure F16 (continued). B. Drawing of general layout of instrument assembly and its position in the left half of the CORK wellhead instrument bay. (**Continued on next page.**)

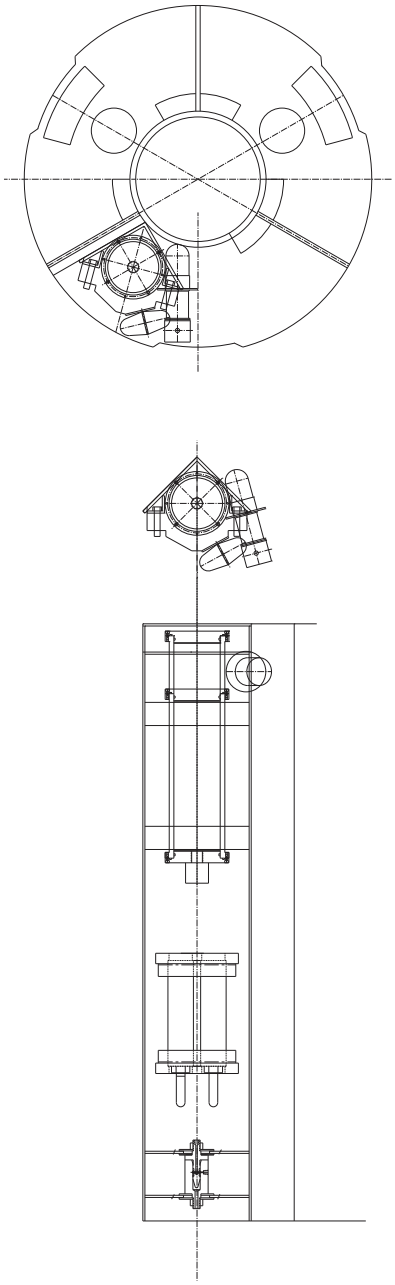

Figure F16 (continued). C. Drawing of mounting frame where the pressure monitoring instrument frame hangs. (**Continued on next page.**)

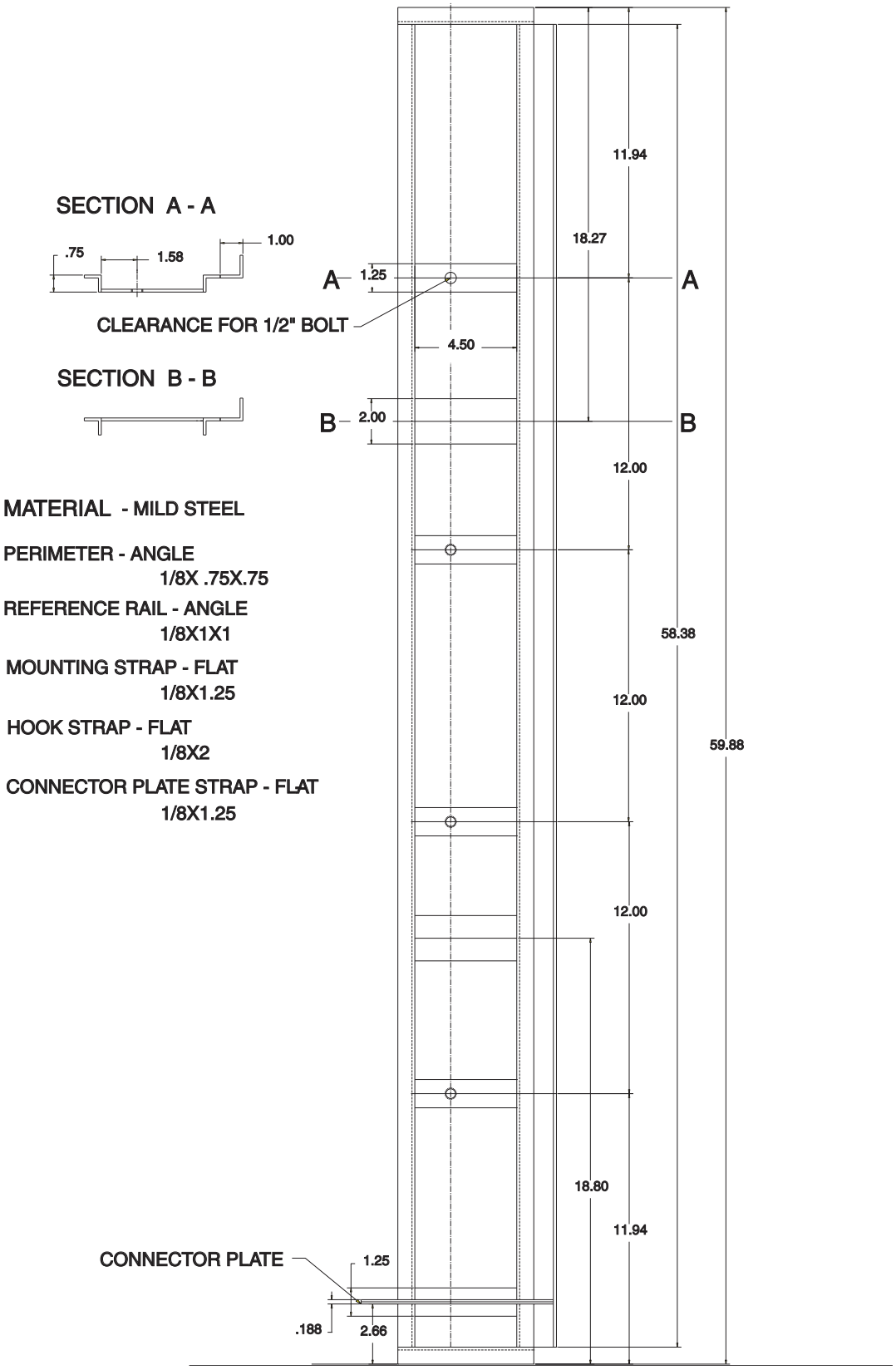

Figure F16 (continued). D. Drawing of bolt pattern for wellhead instrument bay left web, used for temporary bolting of the mounting frame to the wellhead for welding. (**Continued on next page.**)

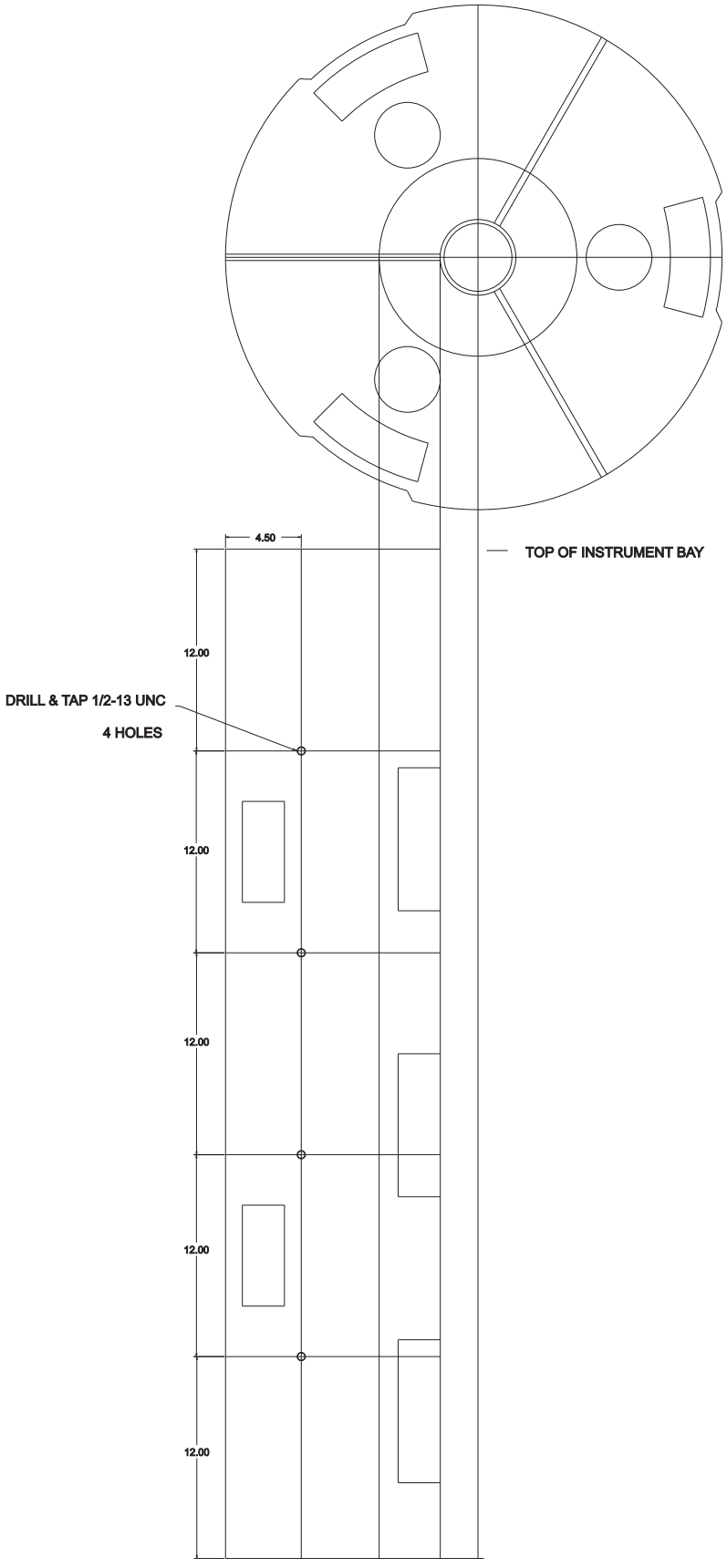

Figure F16 (continued). E. Drawing of pressure-balanced hydraulic couplers. (**Continued on next page.**)

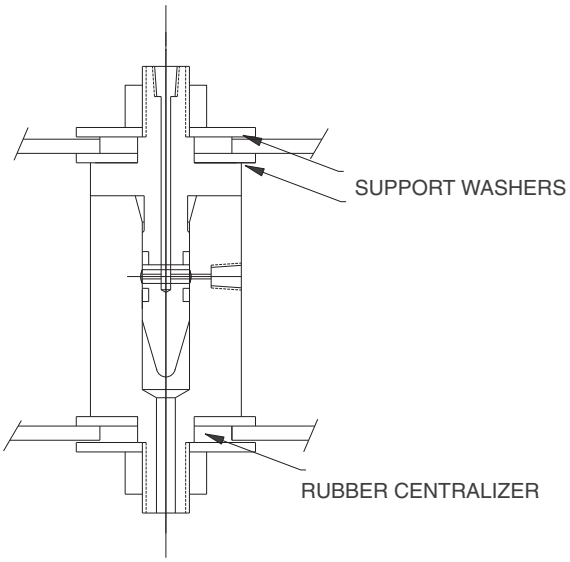

ASSEMBLY

NOTES

- MATERIAL: SS 316
- BREAK ALL EDGES
- ALL DIMENSIONS IN INCHES

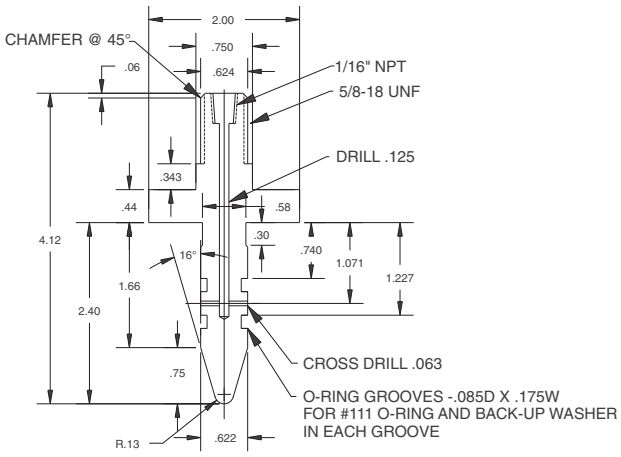

PIN

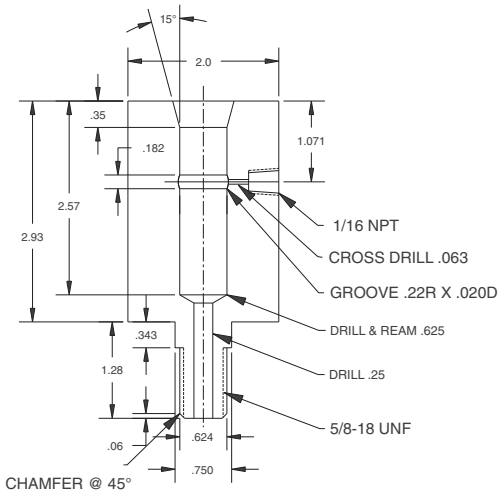

SOCKET

Figure F16 (continued). F. Drawing of mounting pattern for up to four hydraulic coupler pins on base plate of instrument carrier (ordering shown as viewed from above; screen numbers ordered from bottom to top), and for up to four coupler sockets on base plate of wellhead frame. Pairs of intermediate sized holes on instrument carrier base plate hold alignment pins that fit into corresponding holes in wellhead frame base plate, serving as an initial guide for entry of the hydraulic coupler pins into the sockets.

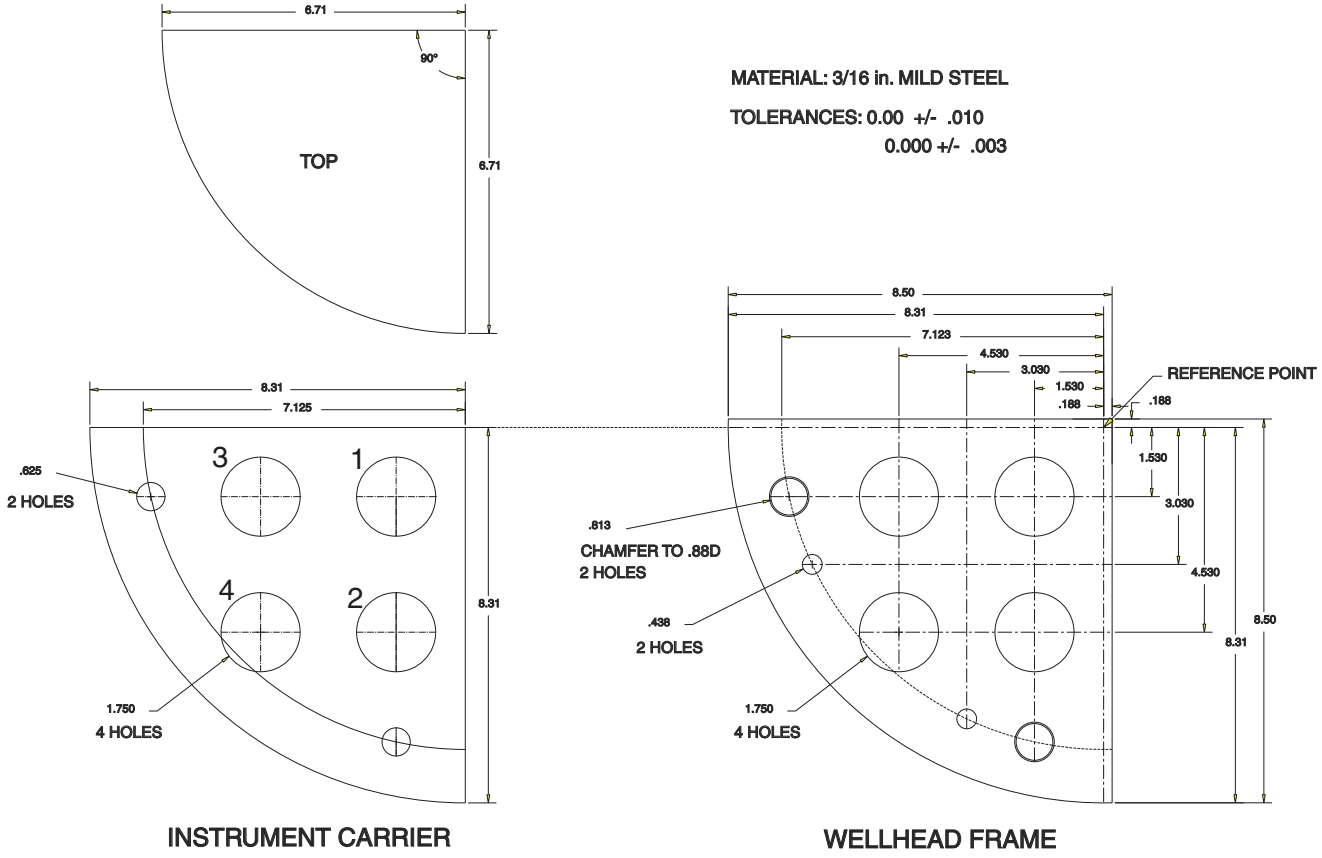

Figure F17. A. Results from plumbing leak test done prior to deployment of the Site U1364 ACORK instrument for lines leading from the umbilical line connections through the wellhead valves to the pressure sensors (see Fig. **F16**). Declines in pressure were the consequence of a slow (~0.1 µL/h) leak in the test supply system. Effects of ship's heave on the ship's water supply are seen prior to closing the supply valve. Response to the quasi-stepwise pressure change at the beginning and end of each test (sole transitional points shown in expanded view in B) demonstrates system frequency response to better than 1 Hz. **B.** Expanded view of A.

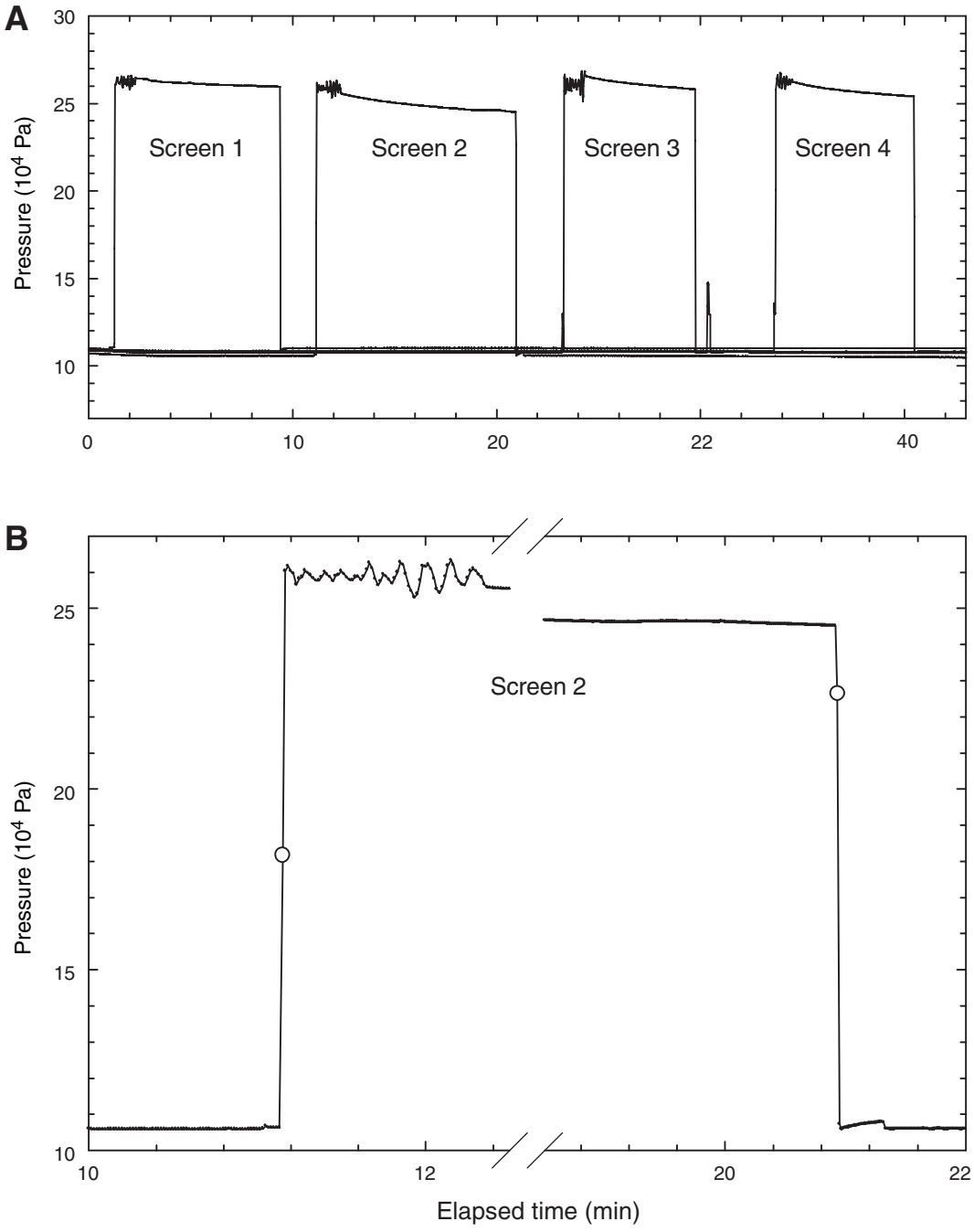

Figure F18. Illustration of the effects of oceanographic and tectonic loading on formation fluid pressure and flow. (Figures after Wang and Davis, 1996; Wang et al., 1998; and Davis et al., 2000.) **A.** Schematic illustration showing response of fluids at pore and formation scales. **B.** Response to loading can be broken into elastic (instantaneous) and diffusive components. **C.** Transients propagate away from a boundary between regions of contrasting elastic properties as a damped diffusive wave with a characteristic scale that depends on permeability. (**Continued on next page.**)

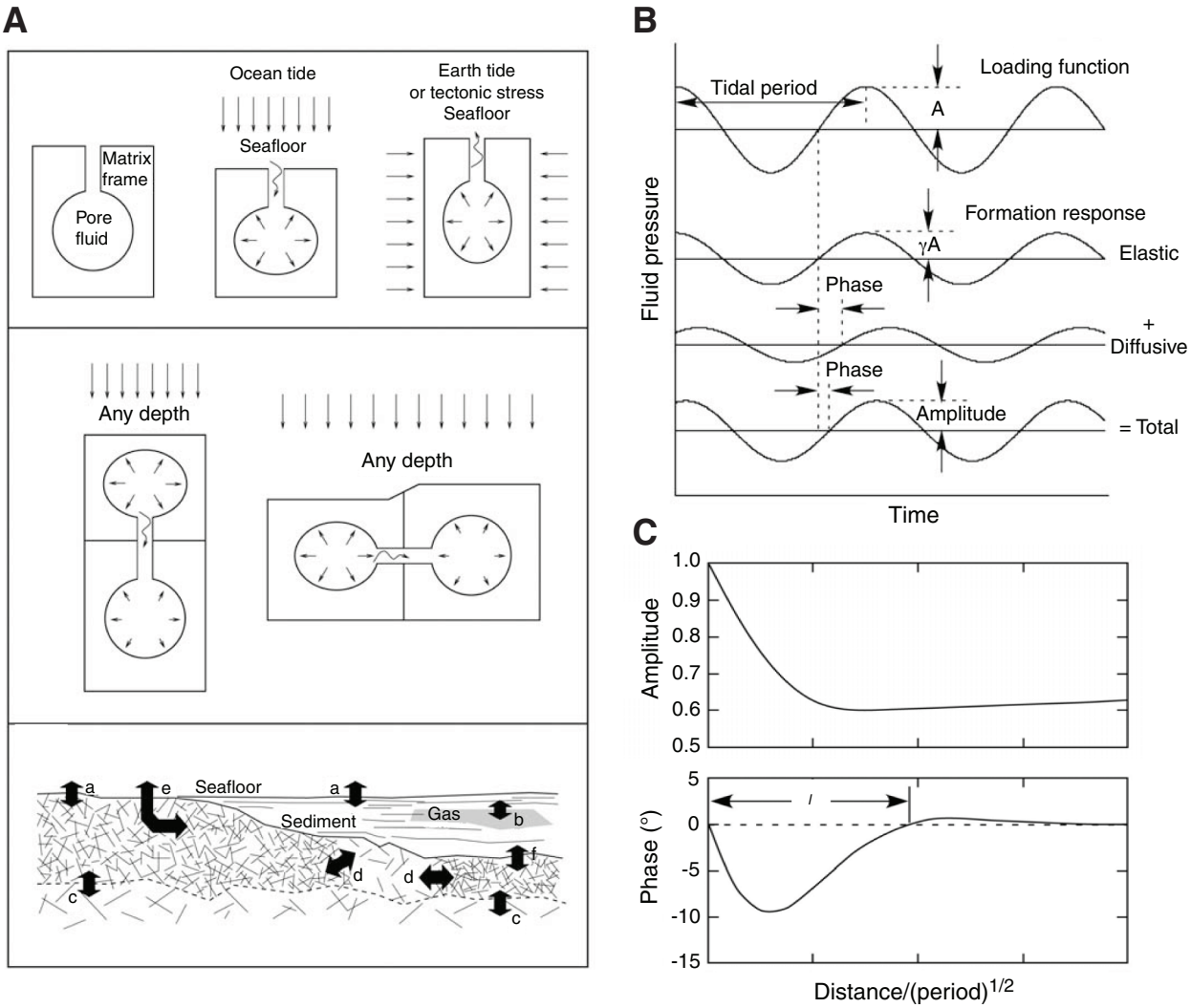

Figure F18 (continued). D. Elastic response expressed as loading efficiency (γ in B) depends on the compressibility of the sediment framework and the compressibility of the interstitial water that may contain free gas. **E.** Response of pressure to volumetric strain in sediment depends primarily on porosity because the compressibility of the matrix is greater than that of water (dotted lines = grain and water compressibilities).

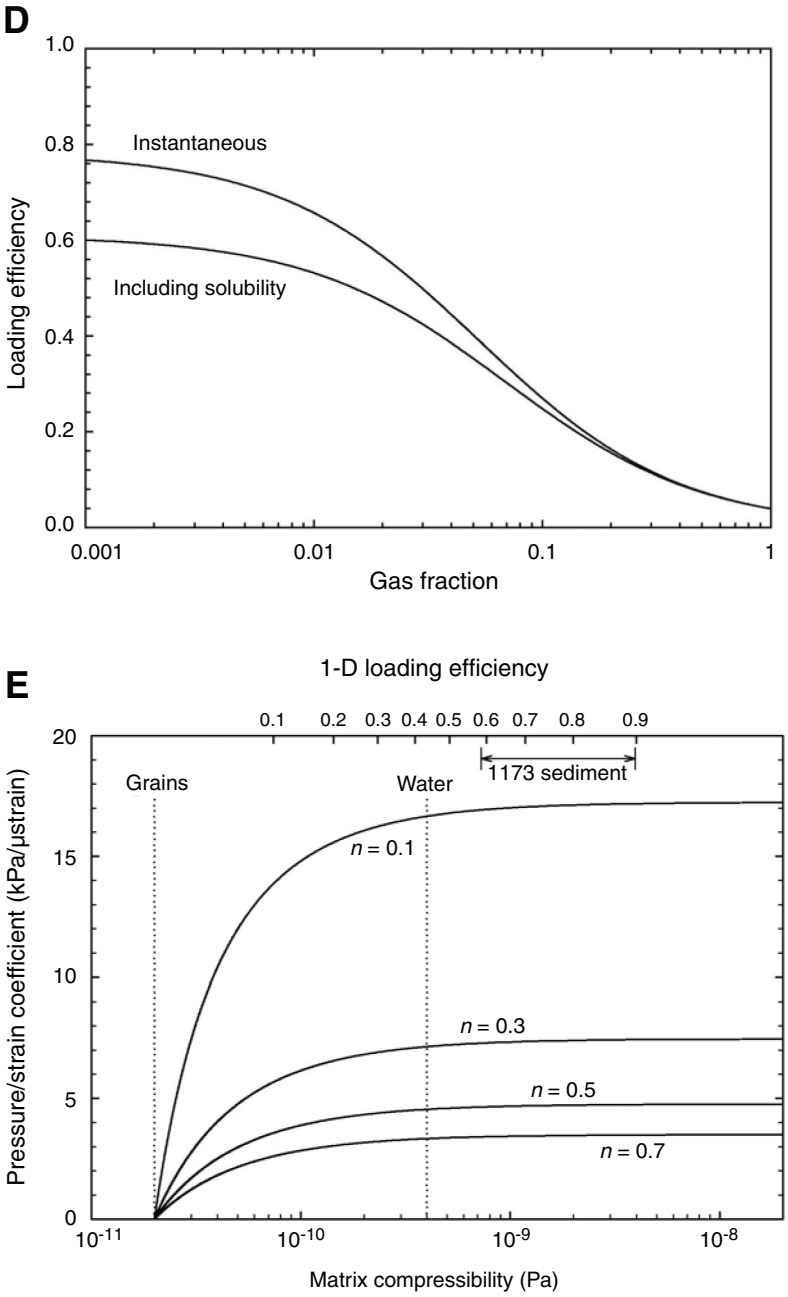

Figure F19. ACORK schematic and installation sequence. Consecutive stages in the installation of the ACORK system includes (**A**) installation of reentry cone and 16 inch diameter conductor casing and drilling 14¾ inch hole to target depth plus a ~15 m rat hole, (**B**) installation of ACORK system with underreamer and mud motor, and (**C**) installation of bridge plug and back-up cement above the casing shoe. Final depths of primary components are given in C. masf = meters above seafloor. CADA = cam-actuated drill-ahead, ROV = remotely operated vehicle.

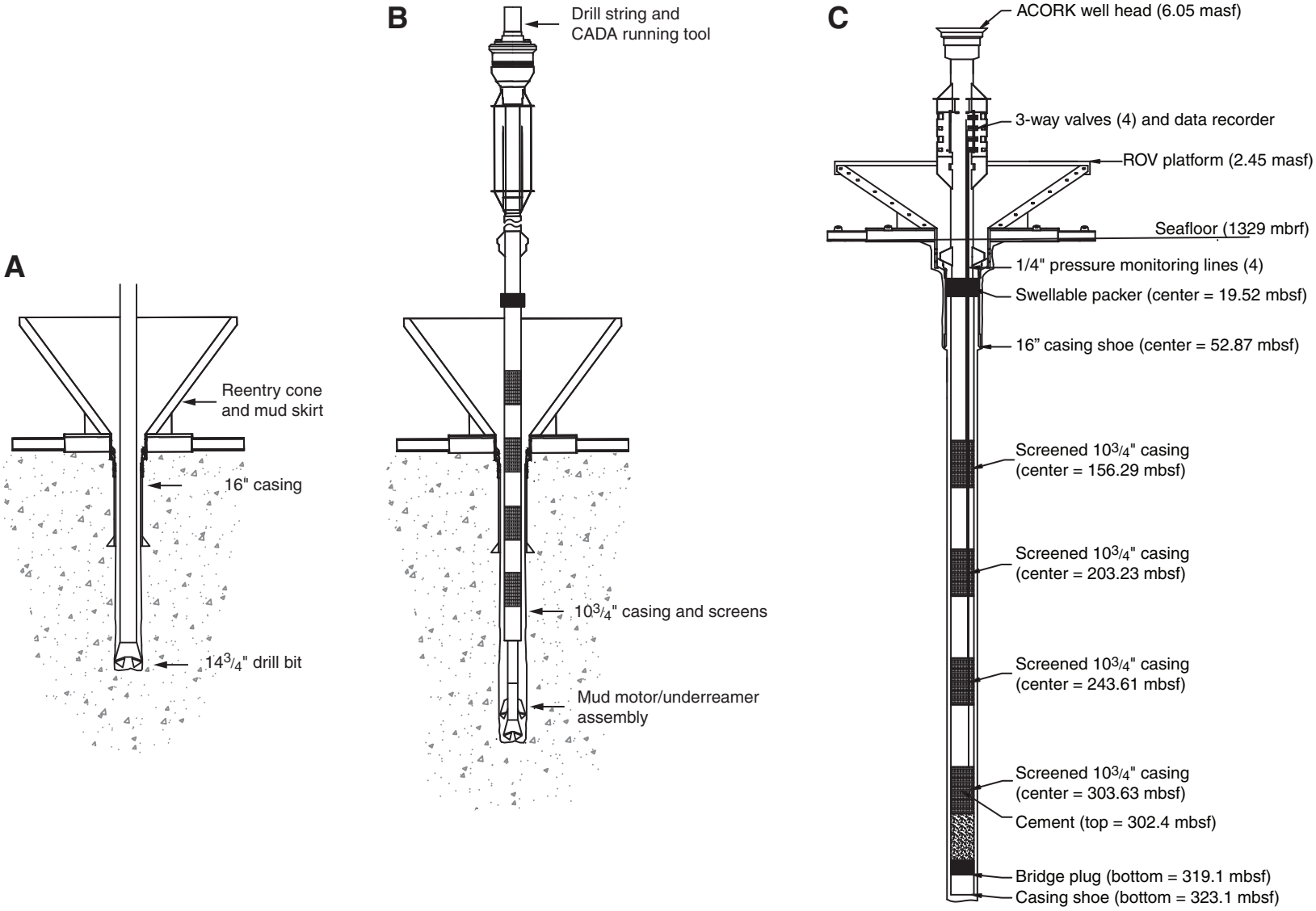

Figure F20. Penetration, penetration rate, and weight on bit data recorded with the Rig Instrumentation System while drilling Hole U1364A with the 14¾ inch drilling assembly.